2005MNRAS.361..725B

Mon. Not. R. Astron. Soc. **361,** 725–742 (2005) doi:10.1111/j.1365-2966.2005.09204.x

Broad-band colours and overall photometric properties of template galaxy models from stellar population synthesis

Alberto Buzzoni★

INAF – Osservatorio Astronomico di Bologna, Via Ranzani 1 - 40127 Bologna, Italy

Accepted 2005 May 16. Received 2005 May 13; in original form 2005 January 20

ABSTRACT

We present here a new set of evolutionary population synthesis models for template galaxies along the Hubble morphological sequence. The models, which account for the individual evolution of the bulge, disc, and halo components, provide basic morphological features, along with bolometric luminosity and colour evolution (including Johnson/Cousins, Gunn g, r, i, and Washington C, M, T_1, T_2 photometric systems) between 1 and 15 Gyr. The luminosity contribution from residual gas is also evaluated, both in terms of nebular continuum and Balmer-line enhancement.

Our theoretical framework relies on the observed colours of present-day galaxies, coupled with a minimal set of physical assumptions related to simple stellar population (SSP) evolution theory, to constrain the overall distinctive properties of galaxies at earlier epochs. A comparison with more elaborate photometric models, and with empirical sets of reference spectral energy distributions (SEDs) for early- and late-type galaxies is accomplished, in order to test output reliability and investigate the internal uncertainty of the models.

The match with observed colours of present-day galaxies tightly constrain the stellar birth rate, b, which smoothly increases from E to Im types. The comparison with the observed supernova (SN) rate in low-redshift galaxies shows, as well, a pretty good agreement, and allows us to tune up the inferred star formation activity and the SN and hypernova rates among the different galaxy morphological types. Among others, these results could find useful application also in cosmological studies, given for instance the claimed relationship between hypernova events and gamma-ray bursts.

One outstanding feature of the back-in-time evolution model is the prevailing luminosity contribution of the bulge at early epochs. As a consequence, the current morphological look of galaxies might drastically change when moving to larger distances, and we discuss here how sensibly this bias could affect the observation (and the interpretation) of high-redshift surveys.

In addition to broad-band colours, the modelling of Balmer line emission in disc-dominated systems shows that striking emission lines, like Hα, can very effectively track stellar birth rate in a galaxy. For these features to be useful age tracers as well, however, one should first assess the real change of b versus time on the basis of supplementary (and physically independent) arguments.

Key words: ISM: lines and bands – galaxies: evolution – galaxies: spiral – galaxies: stellar content.

1 INTRODUCTION

Since its early applications to extragalactic studies (Spinrad & Taylor 1971; Tinsley & Gunn 1978), stellar population synthesis has been the natural tool to probe galaxy evolution. The work of Searle, Sargent & Bagnuolo (1973) and Larson (1975) provided, in this sense, a first important reference for a unified assessment of spectrophotometric properties of early- and late-type systems in the nearby Universe, while the contributions of Bruzual & Kron (1980), Lilly & Longair (1984), and Yoshii & Takahara (1988), among others, represent a pioneering attempt to extend the synthesis approach also to unresolved galaxies at cosmological distances.

In this framework, the colour distribution along the Hubble sequence has readily been recognized as the most direct tracer for

★E-mail: buzzoni@bo.astro.it

© 2005 RAS

© Royal Astronomical Society • Provided by the NASA Astrophysics Data System

2005MNRAS.361..725B

galaxy diagnostics; a tight relationship exists in fact between integrated colours and morphological type, through the relative contribution of bulge and disc stellar populations (Köppen & Arimoto 1990; Arimoto & Jablonka 1991). Ongoing star formation, in particular, is a key mechanism to modulate galaxy colours, especially at short wavelength (Larson & Tinsley 1978; Kennicutt 1998), while visual and infrared luminosity are more sensitive to the global star formation history (Quirk & Tinsley 1973; Sandage 1986; Gavazzi & Scodeggio 1996). External environmental conditions could also play a role, as well as possible interactions of galaxies with embedding giant haloes, like in some CDM schemes (Firmani & Tutukov 1992, 1994; Pardi & Ferrini 1994).

In this work I want to try a simple heuristic approach to galaxy photometric evolution relying on a new family of theoretical template models to account for the whole Hubble morphological sequence. Galaxy evolution is tracked here in terms of the individual history of the composing subsystems, including the bulge, disc and halo; the present discussion completes the analysis already undertaken in an accompanying paper (Buzzoni 2002, hereafter Paper I), and relies on the evolutionary population synthesis code developed previously (Buzzoni 1989, 1995, hereafter B89 and B95, respectively).

A main concern of this work is to provide the user with a quick reference tool to derive broad-band colours and main morphological parameters of galaxies throughout their 'late' evolutionary stages (i.e. for $t \gtrsim 1$ Gyr). This should be the case for most of the $z \lesssim 3$ systems, for which the formation event is mostly over and the morphological design already in place.

Within minor refinements, the present set of models has already been successfully used by Massarotti, Iovino & Buzzoni (2001) in their photometric study of the Hubble Deep Field galaxies; a further application of these templates is also due to Buzzoni et al. (2005), to assess the evolutionary properties of the planetary nebula population in bright galaxies and the intracluster medium. Compared to other more 'physical' (and entangled) approaches, I believe that a major advantage of this simplified treatment is to allow the user to maintain better control of the theoretical output, and get a direct feeling of the changes in model properties as one or more of the leading assumptions are modified.

Models will especially deal with the stellar component, which is obviously the prevailing contributor to galaxy luminosity. Residual gas acts more selectively on the integrated spectral energy distribution (SED) by enhancing monochromatic emission, like for the Balmer lines. As far as galaxy broad-band colours are concerned, in the present age range, its influence is negligible and can be treated separately in our discussion. On the other hand, internal dust could play a more important role, especially at short wavelengths ($\lambda \lesssim 3000$ Å). Its impact for high-redshift observations has been discussed in some detail in Paper I.

In this paper we will first analyse, in Section 2, the basic components of the synthesis model, taking the Milky Way as a main reference to tune up some relevant physical parameters for spiral galaxies. A set of colour fitting functions is also given in this section, in order to provide the basic analytical tool to compute galaxy luminosity for different star formation histories.

Model set-up is considered in Section 3, especially dealing with the physical properties of the disc; metallicity and stellar birth rate will be constrained by comparing with observations and other theoretical studies. In Section 4 we will assemble our template models, providing colours and other distinctive features for each galaxy morphological type along the Hubble sequence, from E to Im. A general sketch of back-in-time evolution is outlined in this section, focusing on a few relevant aspects that deal with the interpretation of high-redshift data. Section 5 discusses the contribution of the residual gas; we will evaluate here the nebular luminosity and derive Balmer emission-line evolution. The main issues of our analysis are finally summarized in Section 6.

2 OPERATIONAL TOOLS

Our models consist of three main building blocks: we will consider a central bulge, a disc, and an external halo. It is useful to track the evolution of each block individually, in terms of composing simple stellar populations (SSPs), taking advantage of the powerful theoretical formalization by Tinsley (1980) and Renzini & Buzzoni (1986).

If SSP evolution is known and a star formation rate (SFR) can be assumed versus time, the general relation for integrated luminosity of a stellar system is

$$L_{\rm gal}(t) = \int_0^t L_{\rm SSP}(\tau)\, {\rm SFR}(t-\tau)\, {\rm d}\tau. \qquad (1)$$

Operationally, the integral in equation (1) is computed in discrete time-steps, $\Delta\tau$, taking the lifetime of the most massive stars in the initial mass function (IMF), $t_{\rm min}$, as a reference, so that $\Delta\tau = t_{\rm min}$.

In a closed-box evolution, the galactic SFR is expected to be a decreasing function of time (e.g. Tinsley 1980; Arimoto & Yoshii 1986); on the other hand, if fresh gas is supplied from the external environment, then an opposite trend might even be envisaged. One straightforward way to account for this wide range of evolutionary paths is to assume a power law such as ${\rm SFR} = K\, t^{-\eta}$, with $\eta < 1$.[1]

As we pointed out in Paper I, an interesting feature of this simple parametrization is that the stellar birth rate,

$$b = \frac{{\rm SFR}(t)}{\langle {\rm SFR} \rangle} = (1-\eta), \qquad (2)$$

is a time-independent function of the SFR and therefore becomes an intrinsic distinctive parameter of the galaxy model.[2]

2.1 SSP evolution

In order to apply equation (1) properly to the different evolutionary cases, we first need to secure its basic 'ingredient' by modelling SSP luminosity evolution. The original set of B89 and B95 population synthesis models, and its following upgrade and extension as in Paper I, especially dealt with evolution of low- and intermediate-mass stars, with $M \lesssim 2$ M$_\odot$ and main sequence (MS) lifetime typically greater than 1 Gyr. As a striking feature in this mass range, red giant branch sets on in stars with a degenerate helium core, tipping at high luminosity ($\log L/{\rm L}_\odot \sim 3.3$) with the so-called helium-flash event (Sweigart & Gross 1978).

For younger ages (i.e. $t \lesssim 1$ Gyr), evolution is less univocally constrained, as convection and mass loss via stellar winds (both depending on metallicity) sensibly modulate the evolutionary path of high-mass stars across the Hertzsprung–Russell (H-R) diagram on time-scales as short as $\sim 10^6$ yr (de Loore 1988; Maeder & Conti

[1] In our notation it must always be that $t \geqslant t_{\rm min}$ as, from equation (1), gas consumption proceeds over discrete time-steps corresponding to the lifetime of high-mass stars.

[2] As the SFR must balance the net rate of change of the residual gas [i.e. ${\rm SFR}(t) = -\dot{g}(t)$], then ${\rm SFR}(t) = (\Delta g/t)(1-\eta)$ and $\langle {\rm SFR} \rangle = t^{-1} \int {\rm SFR}\, {\rm d}\tau = \Delta g/t$. The stellar birth rate $b = (1-\eta)$ can therefore be regarded as an 'efficiency factor' in the gas-to-star conversion.

© Royal Astronomical Society • Provided by the NASA Astrophysics Data System

2005MNRAS.361..725B

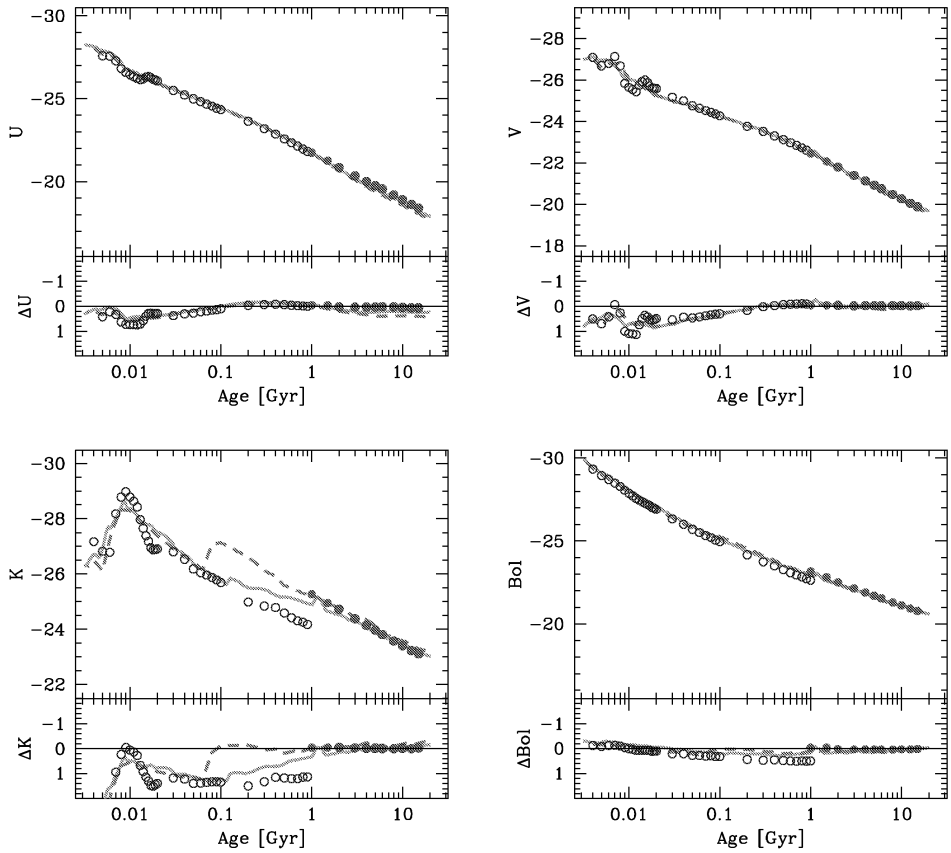

Figure 1. *Upper plots of each panel*: luminosity evolution of present SSP models (solid dots), for solar metallicity and Salpeter IMF, compared with other theoretical outputs according to Leitherer et al. (1999, open dots), Bressan, Chiosi & Fagotto (1994, dashed line), and Bruzual & Charlot (2003, solid line). Total mass is scaled to $M_{\rm SSP} = 10^{11}\,{\rm M}_{\odot}$ throughout, with stars in the range 0.1–120 $\rm M_{\odot}$. The Leitherer et al. (1999) model has been slightly increased in luminosity (by about 0.06 mag in bolometric, at 1 Gyr) to account for the missing luminosity contribution from low-MS stars ($M_{*} \leqslant 1.0\,{\rm M}_{\odot}$). *Lower plots of each panel*: model residuals with respect to the fitting functions of Table 1. See text for discussion.

1994). Such a rapid post-MS evolution could also lead to a biased sampling of stars in the different phases, even at galactic mass-scale, inducing intrinsic uncertainties in the SSP spectrophotometric properties independently of the input details of the physics (see Cerviño et al. 2002 and Cerviño & Valls-Gabaud 2003, for a brilliant assessment of this problem).

A combined comparison of different SSP models, over the full range of stellar masses, is displayed in Fig. 1, where we matched our SSP model sequence for solar metallicity and Salpeter (1955) IMF with the corresponding theoretical output from Bressan, Chiosi & Fagotto (1994), Leitherer et al. (1999) and Bruzual & Charlot (2003, their 'Padova 1994' isochrone set-up). Luminosity in the Johnson *U*-, *V*-, *K*-bands, and also the bolometric luminosity, is shown in the four panels of the figure, referring to the evolution of a $10^{11}\,{\rm M}_{\odot}$ SSP, with stars in the range $0.1 \leqslant M_{*}/{\rm M}_{\odot} \leqslant 120$. To compare consistently with the other outputs, the Leitherer et al. models have been slightly increased in luminosity (by some $\Delta{\rm mag} = -0.06$ in bolometric at 1 Gyr) to account for the missing low-MS ($M_{*} < 1\,{\rm M}_{\odot}$) contribution, according to the B89 estimates.

Fig. 1 shows a remarkable agreement between the four theoretical codes; in particular, ultraviolet and bolometric evolution is fairly well tracked over nearly four orders of magnitude of SSP age. The lack of asymptotic giant branch (AGB) evolution in the Leitherer et al. (1999) code is, however, especially evident in the *K* plot, where a glitch of about 1 mag appears at the match with our model sequence about $t \sim 1$ Gyr. To a lesser extent, also the *K*-band contribution of red giant stars seems to be partly undersized in the Bruzual & Charlot (2003) models between 10^{8} and 10^{9} yr, probably due to interpolation effects across stellar tracks in the relevant range of mass (i.e. $M_{*} = 5 \rightarrow 2\,{\rm M}_{\odot}$).

Definitely, SSP evolution appears to be best tracked by the isochrone-synthesis models of Bressan et al. (1994); like in our code, these models meet the prescriptions of the so-called 'fuel consumption theorem' (Renzini & Buzzoni 1986), and self-consistently account for the AGB energetic budget down to the onset of supernova (SN) II events (about $t \simeq 10^{8}$ yr). In any case, as far as early SSP evolution is concerned, a combined analysis of Fig. 1 makes clear the intrinsic uncertainty of the synthesis output in this particular age range, mainly as a result of operational and physical differences in the treatment of post-MS evolution (cf. Charlot, Worthey & Bressan 1996, for further discussion on this subject).

2.2 SSP fitting functions

Model set-up, like in case of composite stellar populations according to equation (1), would be greatly eased if we could manage the problem semi-analytically, in terms of a suitable set of SSP magnitude-fitting functions. An important advantage in this regard is that also intermediate cases for age and/or metallicity could readily be accounted for in our calculations.

For this task we therefore considered the B89 and B95 original data set of SSP models (and its further extension, as in Paper I),

© Royal Astronomical Society • Provided by the NASA Astrophysics Data System

2005MNRAS.361..725B

Table 1. SSP magnitude fitting functions for a Salpeter IMF with stars in the mass range $0.1 \leqslant M/M_{\odot} \leqslant 120$.

Band	$\lambda_{\rm eff}$	$\log f_{\rm o}^{(a)}$	mag $= (\alpha' + \alpha''$ [Fe/H]) $\log t_9 + \beta$ [Fe/H] $+ \gamma + \delta$(t $_9$, [Fe/H])					σ	System
	(Å)	(erg s^{-1} cm^{-2} Å^{-1})	α'	α''	β	γ	δ(t$_9$, [Fe/H])	(mag)	
U	3650	−8.392	2.743	0.26	0.006	2.872	$+0.09\,10^{[Fe/H]}$	±0.026	Johnson
C	3920	−8.275	2.560	0.16	−0.024	2.853	$+0.09\,10^{[Fe/H]}$	±0.022	Washington
B	4420	−8.205	2.390	0.08	0.033	2.909		±0.020	Johnson
M	5060	−8.351	2.232	0.08	−0.060	2.477		±0.020	Washington
g	5170	−8.384	2.214	0.08	−0.069	2.401		±0.019	Gunn
V	5500	−8.452	2.163	0.08	−0.094	2.246		±0.019	Johnson
T_1	6310	−8.632	2.072	0.08	−0.160	1.835		±0.019	Washington
$R_{\rm C}$	6470	−8.670	2.048	0.08	−0.176	1.756		±0.019	Cousins
r	6740	−8.527	2.037	0.08	−0.189	2.147		±0.019	Gunn
R	7170	−8.790	2.006	0.08	−0.207	1.546		±0.019	Johnson
$I_{\rm C}$	7880	−8.936	1.977	0.08	−0.275	1.226		±0.019	Cousins
T_2	7940	−8.938	1.972	0.08	−0.255	1.250		±0.019	Washington
i	8070	−8.653	1.969	0.08	−0.259	1.981		±0.019	Gunn
I	9460	−9.136	1.923	0.08	−0.327	0.944		±0.020	Johnson
J	12500	−9.526	1.863	0.08	−0.444	0.333		±0.018	Johnson
H	16500	−9.965	1.833	0.08	−0.551	−0.375		±0.016	Johnson
K	22000	−10.302	1.813	0.08	−0.614	−0.561		±0.016	Johnson
Bol			1.923		−0.324	1.623	$-0.1\,t_9^{-0.5}$	±0.014	

[a] $\log f = -0.4\,{\rm mag} + \log f_{\rm o}$. For the bolometric: $\log L/L_{\odot} = -0.4({\rm Bol} - 4.72)$

.

with the Salpeter IMF and red horizontal branch morphology (cf. B89 for details). In addition to the original Johnson photometry, we also included here the Cousins ($R_{\rm C}$, $I_{\rm C}$), Gunn (g, r, i), and Washington (C, M, T_1, T_2) band systems. The work of Canterna (1976), Thuan & Gunn (1976), Bessell (1979) and Schneider, Gunn & Hoessel (1983) has been referred to for the different system definitions (see also Cellone & Forte 1996, for an equivalent calibration of the Washington colours based on the B89 models). Our analysis will therefore span a wide wavelength range, from 3600 Å (U-band), to 2.2 μm (K-band), sampling SSP luminosity at roughly $\Delta\,\lambda \sim$ 400 Å steps in the spectral window between 3600 and 9000 Å.

For SSP magnitude evolution, a general fit was sought in the form

$$\mathrm{mag} = (\alpha' + \alpha''\,[\mathrm{Fe/H}])\ \log t_9 + \beta\,[\mathrm{Fe/H}] + \gamma + \delta(\mathrm{t}_9, [\mathrm{Fe/H}]), \tag{3}$$

where t_9 is the SSP age, expressed in Gyr. The whole set of fitting coefficients is summarized in Table 1 (columns 4–8); note that the U magnitude scale in the table already accounts for the corrections devised in B95. Column 2 of the table reports the effective wavelength for each photometric passband, as directly computed from the adopted filter profile.

Mass scaling for the SSP fitting functions in Table 1 can be done by adding to all magnitudes an offset

$$\Delta\mathrm{mag} = -2.5 \log M_{\rm tot} + 2.5 \log(M/L_V)_{15}, \tag{4}$$

where both SSP total mass and the V-band mass-to-light ratio (estimated at $t = 15$ Gyr) are in solar units. A quite accurate fit (within a ±1.5 per cent relative scatter) for the latter quantity over the metallicity range of our models is:

$$\left(\frac{M}{L_V}\right)_{15} = 3.23\,([\mathrm{Fe/H}] + 1.5)^2 + 6.41. \tag{5}$$

Again, the fit holds for stars in the range 0.1–120 $M_{\odot}$ and a Salpeter IMF.

The whole set of fitting functions in Table 1 is optimized in the range $[\mathrm{Fe/H}] = [-1.5, +0.5]$. For $t \geqslant 1$ Gyr, the model grid is fitted with an internal accuracy better than ±0.02 mag, slightly worsening in the ultraviolet, as reported in column 9 of the table.

The residual trend of the Bressan et al. (1994), Leitherer et al. (1999) and Bruzual & Charlot (2003) SSP models with respect to our fitting functions is displayed in the lower plot of each panel of Fig. 1. Reference equations give a fully adequate description of SSP luminosity evolution well beyond the nominal age limits of our model grid, and span the whole range of AGB evolution, for $t \geqslant 10^8$ yr. At early epochs, of course, fit predictions partially miss the drop in the SSP integrated luminosity, when core-collapsed evolution of high-mass stars ends up as a SN burst thus replacing the standard AGB phase (we will return to this important feature in Section 4.1). As far as composite stellar populations are concerned, however, the induced uncertainty of fit extrapolation on the total luminosity of the system is much reduced since equation (1) averages SSP contribution over time.[3]

3 MODEL SET-UP: THE BASIC BUILDING BLOCKS

To assemble the three main building blocks of our synthesis models consistently we mainly relied on the Kent (1985) galaxy decomposition profiles, which probe the spheroid (i.e. bulge+halo) versus disc luminosity contribution at red wavelengths (Gunn r-band). Kent's results substantially match also the near-infrared observations (see Fig. 2), while B luminosity profiles (Simien & de Vaucouleurs 1986)

[3] For the illustrative case of a SFR constant in time, from our calculations we estimate that the effect of the 'AGB glitch' in the first 10^8 yr of SSP evolution, with respect to a plain extrapolation of Table 1 fitting functions, is reflected in the integrated colours of the composite stellar population by $\Delta(B-V) \simeq \Delta(V-K) \lesssim 0.06$ mag for 1 Gyr models. In terms of absolute magnitude, the luminosity drop amounts to a maximum of ∼0.25 mag in the K-band, at 1 Gyr (and for $\eta = 0$), reducing to a $\Delta K \simeq 0.1$ mag for 15-Gyr models. All these figures will further reduce at shorter wavelength and when the SFR decreases with time (i.e. for $\eta > 0$); they could be taken, therefore, as a conservative upper limit to the internal uncertainty of our models. In any case, in this work we will restrain our analysis only to galaxies older than 1 Gyr.

© Royal Astronomical Society • Provided by the NASA Astrophysics Data System

2005MNRAS.361..725B

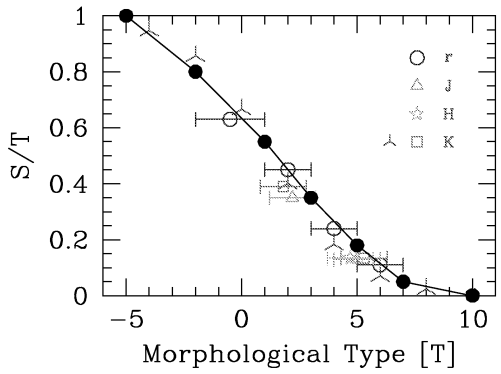

Figure 2. The adopted red/infrared calibration for the S/T morphological parameter, defined as $L_{\rm spheroid}/L_{\rm tot}$ (• markers), as derived from the data of Kent (1985; ○ markers), de Jong (1996; reversed 'Y' markers), Giovanardi & Hunt (1988; □, △ and ⋆ markers for later-type spirals at $T \sim 5$), and Moriondo, Giovanardi & Hunt (1998; △ and □ markers for early-type spirals, about $T \sim 2$). Photometric bands of observations are labelled top right in the plot.

tend in general to show a slightly enhanced disc component in later-type spirals, as a consequence of a bluer colour with respect to the bulge.

For each Hubble type we eventually calibrated a morphological parameter defined as S/T = L (spheroid)/L(tot). As the S/T calibration does not vary much at visual and infrared wavelength, we fixed the I luminosity as a reference for model set-up. This also traces the bolometric partition (cf. the corresponding fitting coefficients of Table 1) fairly well, especially for early-type spirals. According to the observations, the luminous mass of the disc remains roughly constant along the Sa–Im sequence, while bulge luminosity decreases towards later-type spirals (Simien & de Vaucouleurs 1983; Gavazzi 1993).

3.1 The spheroid subsystem

There is a general consensus on the fact that both the halo and bulge subsystems in the Galaxy basically fit with coeval SSPs older than ∼13 Gyr (Gilmore, King & van der Kruit 1990; Renzini 1993; Frogel 1999; Feltzing & Gilmore 2000). Observations of the central bulge of the Milky Way show that it mostly consists of metal-rich stars (Frogel 1988, 1999) and this seems a quite common situation also for external galaxies (Jablonka, Martin & Arimoto 1996; Goudfrooij, Gorgas & Jablonka 1999; Davidge 2001). The exact amount of bulge metallicity, however, has been subject to continual revision in recent years, ranging from a marked metal overabundance (i.e. [Fe/H] ∼ +0.2; Whitford & Rich 1983; Rich 1990; Geisler & Friel 1992) to less prominent values, actually consistent with a standard or even slightly subsolar metallicity (Tiede, Frogel & Terndrup 1995; Sadler, Rich & Terndrup 1996; Zoccali et al. 2003; Origlia & Rich 2005).

On the other hand, the halo mostly consists of metal-poor stars (Zinn 1980; Sandage & Fouts 1987), and its metallicity can be probed by means of the globular cluster environment. From the complete compilation of 149 Galactic globular clusters by Harris (1996), for instance, we derive a mean [Fe/H] = -1.24 ± 0.56, with clusters spanning a range $-2.3 \lesssim$ [Fe/H] $\lesssim 0.0$. This figure is in line with the inferred metallicity distribution of globular cluster systems in external galaxies (Brodie & Huchra 1991; Durrell et al. 1996; Perrett et al. 2002; Kissler-Patig et al. 2003).

According to the previous arguments, for the spheroid component in our models we will adopt two coeval SSPs with [Fe/H] = +0.22 and −1.24, for bulge and halo, respectively.[4] Once we account for metallicity, via equation (5) and Table 1, the standard halo/bulge mass ratio for the Milky Way (e.g. Sandage 1987; Dwek et al. 1995) translates into a relative bolometric luminosity:

$$[L_{\rm halo} : L_{\rm bulge}] = [15\% : 85\%]. \quad (6)$$

This partition will be adopted throughout in our models and provides a nearly solar luminosity-weighted metallicity for the spheroid system as a whole.

3.2 The disc

To set the distinctive parameters of the disc we need to constrain suitably the stellar birth rate, b (or, equivalently, the SFR power-law index, η), and mean stellar metallicity along the Hubble morphological sequence. This could be done by relying on the observed colours of present-day galaxies. In our analysis we will assume a current age of 15 Gyr.

The most exhaustive collection of photometric data for local galaxies definitely remains the RC3 catalog (de Vaucouleurs et al. 1991). Based on the original data base of over 2500 objects, Buta et al. (1994) carried out a systematic analysis of the optical colour distribution. Another comprehensive compilation from the RC3-UGC catalogs (1537 galaxies in total) is that of Roberts & Haynes (1994). Both data samples have been extensively discussed in Paper I; their analysis shows that a 1σ colour scatter of the order of ± 0.15 mag can be devised both for the $B-V$ and $U-B$ distributions as a realistic estimate of the intrinsic spread within each T morphology class (cf. also Fukugita, Shimasaku & Ichikawa 1995, on this point). This value should probably be increased by a factor of 2 for the infrared colours.

3.2.1 Two-colour diagrams and disc metallicity

A two-colour diagram is especially suitable to constrain disc metallicity. Our experiments show in fact that any change in the stellar birth rate will shift the integrated colours along the same mean locus, for a fixed value of [Fe/H]. In Fig. 3, a set of disc model sequences with varying metallicity is compared with the U, B, V, K photometry from the work of Pence (1976), Aaronson (1978), Gavazzi, Boselli & Kennicutt (1991), and Buta et al. (1994). We only included those data samples with complete multicolour photometry, avoiding combining colours from different sources in the literature. The theoretical loci in the figure have been computed by adding to the same spheroid component an increasing fraction of disc luminosity, according to equation (1) and assuming a SFR with $\eta = -0.8$. Three values for metallicity have been considered, namely [Fe/H] = 0.0, −0.5 and −1.0 dex.

Both the $(U-V)$ versus $(V-K)$ and $(U-B)$ versus $(B-V)$ plots clearly point to a mean subsolar metal content for the disc stellar component. This is especially constrained by late-type galaxies, where the disc dominates the total luminosity. We could tentatively adopt $[{\rm Fe/H}]_{\rm disc} = -0.5$ dex as a luminosity-weighted representative value for our models.[5] As pointed out in Paper I, this

[4] We chose to maintain a super-solar metallicity for the bulge component, in better agreement with the observations of external galaxies.

[5] In the case of continual star formation, the luminosity-weighted 'mean' metallicity of a composite stellar population is in general lower than the actual [Fe/H] value of the youngest stars (and residual gas). This is because of the relative photometric contribution of the metal-poor unevolved component of low-mass stars, which biases the mean metal abundance toward lower values.

© Royal Astronomical Society • Provided by the NASA Astrophysics Data System

2005MNRAS.361..725B

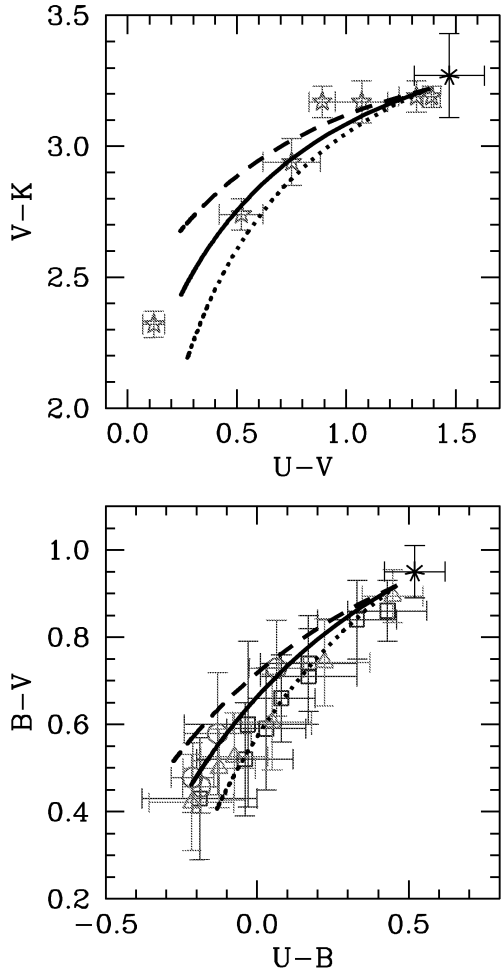

Figure 3. Two-colour diagrams of galaxy distribution compared with 15-Gyr model sequences for different values of disc metallicity. Data are from Aaronson (1978, ⋆ markers), Pence (1976, ○), Gavazzi et al. (1991, □), and Buta et al. (1994, △). Mean colours for ellipticals (the ∗ marker in each panel) are from B95. In the models, a disc component is added as an increasing fraction of the total galaxy luminosity (in the sense of increasingly bluer colours). Long-dashed line is the theoretical locus for solar metallicity, while solid and dotted lines are for $[\,\mathrm{Fe/H}\,]_{\mathrm{disc}} = -0.5$, and -1.0 dex, respectively.

value roughly agrees with the Milky Way stellar population in the solar neighbourhood (Edvardsson et al. 1993), and is in line with the theoretical estimates of Arimoto & Jablonka (1991), suggesting a mean luminosity-weighted $[\mathrm{Fe/H}]_{\mathrm{disc}} \sim -0.3$ dex for their disc-dominated galaxy models. The intrinsic spread of the observations in Fig. 3, compared with the full range of the [Fe/H] loci, indicates, however, that metal abundance is not a leading parameter to modulate disc colours, and even a ± 0.3 dex change in our assumptions would not seriously affect model predictions.

3.2.2 Colour distribution and disc SFR

Colour distribution along with the S/T morphological parameter is a useful tool to constrain the disc SFR. This plot is in fact more sensitive to the relative amount of young versus old stars in the galaxy stellar population, and gives an implicit measure of the disc birth rate, *b*. Our results are summarized in Fig. 4, compared with the available *UBV* photometry.

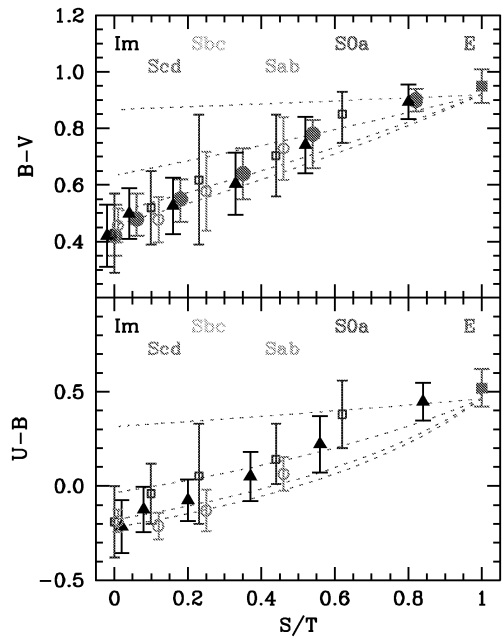

Figure 4. Galaxy colour distribution versus bolometric morphological parameter $\mathrm{S/T} = L_{\mathrm{spheroid}}/L_{\mathrm{tot}}$ compared with 15-Gyr model sequences with fixed SFR power-law index. Data are from Pence (1976, ○ markers), Gavazzi et al. (1991, □), Roberts & Haynes (1994, •), and Buta et al. (1994, ▲). Mean colours for ellipticals (■) are from B95. Dotted lines display the expected locus for models with three different values of the SFR index, namely $\eta = -0.8$, 0, and $+0.8$ plus the SSP case, in the sense of increasingly redder colours. A trend is evident in the observations with a higher stellar birth rate for later-type systems.

Four model sequences are displayed in each panel according to three different values of the SFR power-law index, namely $\eta = 0.8$, 0.0, -0.8 (i.e. $b = 0.2$, 1, 1.8) plus the case of a plain SSP evolution. We adopted $[\mathrm{Fe/H}]_{\mathrm{disc}} = -0.5$ dex throughout in our calculations. Both the $B-V$ and $U-B$ plots indicate, in average, a higher stellar birth rate for later-type systems (Kennicutt, Tamblyn & Congdon 1994). Our adopted calibration for *b* versus morphological type is shown in fig. 8 of Paper I.

It is useful to compare our final results with the models of Arimoto & Jablonka (1991), which addressed disc chemio-photometric evolution in more detail. Slightly different IMF boundaries were adopted by Arimoto & Jablonka (1991) (i.e. a power-law index $s = 2.45$ instead of our standard Salpeter value, $s = 2.35$, and a stellar mass range $M_* = [0.05, 60]\,\mathrm{M}_\odot$ versus our value of $M_* = [0.1, 120]\,\mathrm{M}_\odot$), so that we had to rescale their original values to consistently compare with our M/L ratio. Fig. 5 shows remarkable agreement with our results, along the whole late-type galaxy sequence, both in terms of integrated colours and stellar M/L ratio. To account for the missing luminosity of 60–120 $\mathrm{M}_\odot$ stars in the Arimoto & Jablonka (1991) models, however, one should further decrease the inferred M/L ratio for their output in Fig. 5, especially for Sc–Sd systems.

4 MODEL OUTPUT

The distinctive parameters eventually adopted for our galaxy templates, according to the previous discussion, have been collected in Table 2. A synoptic summary of the main output properties for 15- and 1-Gyr models is reported in Table 3. Compared with the

© Royal Astronomical Society • Provided by the NASA Astrophysics Data System

2005MNRAS.361..725B

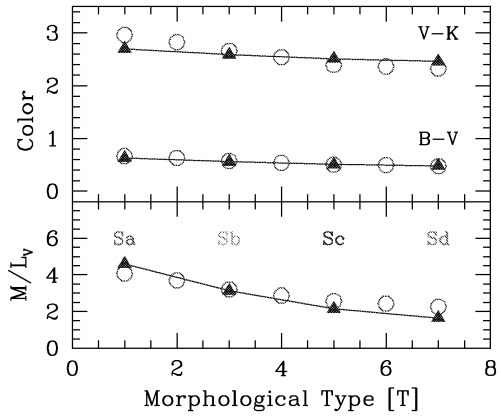

Figure 5. Comparison of our disc model output (▲ markers) versus the Arimoto & Jablonka (1991) original results (○ markers). The V-band M/L ratio (in solar units) refers to the stellar mass alone (i.e. the total mass converted to stars at the age of 15 Gyr); it has been normalized consistently, to account for the slightly different IMF mass range and slope (see text for discussion).

Table 2. Distinctive input parameters for 15-Gyr models.

Hubble type	$b^{(a)}$	η	S/T$^{(b)}$	[Fe/H] [halo : disc : bulge]
E	0.0	SSP	1.00	−1.24 +0.22
S0	0.0	SSP	0.80	−1.24 −0.50 +0.22
Sa	0.2	0.8	0.55	−1.24 −0.50 +0.22
Sb	0.5	0.5	0.35	−1.24 −0.50 +0.22
Sc	0.9	0.1	0.18	−1.24 −0.50 +0.22
Sd	1.3	−0.3	0.05	−1.24 −0.50 +0.22
Im	1.8	−0.8	0.00	−0.50

[a]Disc stellar birth rate.
[b]S/T = L(spheroid)/L (tot) at red/infrared wavelength.

models of Paper I, notice that we slightly revised here the bolometric luminosity scale as a consequence of a refined fitting function in Table 1. We therefore predict here a lower bolometric M/L ratio (because of a higher $L_{\rm bol}$ value), compared to table 3 of Paper I. Apart from this difference, the change has no effect on the rest of the model properties as bolometric luminosity is a *derived* quantity for our calculations; full consistency is therefore preserved with the framework of Paper I.

Template galaxy models are described in full detail in the series of Tables A1–A7 of Appendix A, assuming a total mass $M_{\rm gal} = 10^{11}\,{\rm M}_\odot$ for the system at 15 Gyr.[6] In addition to the standard colours in the Johnson, Gunn and Washington photometric systems, also 'composite' colours like $(g - V)$ and $(M - V)$ are reported in the tables in order to allow an easier transformation of photometry among the different systems. It could also be useful to recall, in this regard, that a straightforward transformation of the Johnson/Cousins magnitudes to the Sloan SDSS (u', g', r', i', z') photometric system can be obtained by relying on the set of equations in Fukugita et al. (1996, their equation 23). A plot of the synthetic SED for 15-Gyr galaxies is displayed in Fig. 6 in a log–log plot. The luminosity at different wavelengths is obtained by converting theoretical magnitudes to absolute apparent flux, according to the photometric zero-points of Table 1 (column 3). In the figure, ultraviolet magnitudes at 1600, 2000 and 2800 Å are from Paper I.

A comparison of our output with the empirical SED for template galaxies along the Hubble sequence is carried out in Fig. 7. Mean reference spectra are those assembled by Coleman, Wu & Weedman (1980) for types E (the M81 case), Sbc, Scd, and Im, while the SED of the Sab type in the figure is from Pence (1976). From the plots one can appreciate a fully suitable match between observed and theoretical SED longward of the U-band. Two interesting features, however, are worthy of attention, for a deeper analysis: (i) empirical templates (especially for spirals) always display a 'depressed' ultraviolet emission, compared to the theoretical SED; (ii) the Im empirical template more closely fits a young (∼5 Gyr) theoretical model.

As we have further discussed in Paper I, point (i) is the obvious signature of dust in the SED of real galaxies. Although this effect is not explicitly taken into account in our models, it could easily be assessed in any *ex post* analysis of the observations by adopting a preferred shape for the attenuation curve to correct the data, as proposed, for example, in the studies of Bruzual, Magris & Calvet (1988) and Calzetti (1999). In any case, as previously mentioned, it is evident from Fig. 7 that dust effects only enter at the very short-wavelength range ($\lambda \lesssim 3000$ Å) of the galaxy SED. Finally, as for point (ii) above, one has to recall that the Coleman et al. (1980) reference template for the Im-type relies on just one 'extremely blue irregular galaxy' (i.e. NGC 4449). For this target, the authors report, as integrated colours, $(U - V) = -0.06$ and $(B - V) = 0.32$, placing the object in the extreme blue range of the typical colours for irregulars (see, for instance, Figs 3 and 4, and also the relevant discussion by Fukugita et al. 1995); a younger age is therefore required to match the observed SED for this galaxy.

4.1 Supernova and hypernova rates

A natural output of template models deals with the current formation rate of core-collapsed stellar objects. This includes types II/Ibc supernovae and their hypernova (HN) variant (Paczynski 1998) for very high-mass stars. Both the SN and HN events are believed to originate from the explosion of single massive stars and have therefore a direct link with the galaxy stellar birth rate. Hypernovae, in particular, have recently become a central issue in the investigation of extragalactic gamma-ray bursts (Nakamura et al. 2000; Woosley & MacFayden 2000).

If we assume, with Bressan et al. (1994), that all stars with $M_* \geqslant 5\,{\rm M}_\odot$ eventually undergo an explosive stage, and those more massive than $40\,{\rm M}_\odot$ generate a hypernova burst (Iwamoto et al. 1998), then the number of SN(II+Ibc)+HN events in a SSP of total mass $M_{\rm SSP}$ (in solar units) and Salpeter IMF can be written as:

$$N_{\rm SN+HN} = \frac{0.35}{1.35}\left(\frac{5^{-1.35} - 120^{-1.35}}{0.1^{-0.35} - 120^{-0.35}}\right) M_{\rm SSP} = 0.0142\, M_{\rm SSP} \quad [{\rm M}_\odot^{-1}]. \tag{7}$$

The expected fraction of SN(II+Ibc) relative to HN candidates, for a Salpeter IMF is,

$$[N_{\rm SN} : N_{\rm HN}] = [20 : 1]. \tag{8}$$

If disc SFR does not change much on a time-scale comparable with the lifetime of 5-${\rm M}_\odot$ stars (i.e. $\sim 10^8$ yr), then a simplified

[6] Throughout this paper, $M_{\rm gal}$ refers to the amount of mass converted to stars (that is, $M_{\rm gal} = \int {\rm SFR}\, {\rm d}t$) and therefore it does *not* include residual gas. By definition, $M_{\rm gal}$ increases with time.

© Royal Astronomical Society • Provided by the NASA Astrophysics Data System

Table 3. Output summary for template galaxy models at 1 and 15 Gyr.

	1 Gyr								15 Gyr							
Hubble Type	S/T[a]	L/L_{tot}[b] [halo : disc : bulge]			M/M_{tot}[c] [halo : disc : bulge]			M/L[d]	S/T	L/L_{tot} [halo : disc : bulge]			M/M_{tot} [halo : disc : bulge]			M/L
E	1.00	0.15	0.00	0.85	0.09	0.00	0.91	0.74	1.00	0.15	0.00	0.85	0.09	0.00	0.91	6.41
S0	0.81	0.12	0.19	0.69	0.08	0.16	0.76	0.71	0.81	0.12	0.19	0.69	0.08	0.16	0.76	6.14
Sa	0.66	0.10	0.34	0.56	0.08	0.17	0.75	0.59	0.52	0.08	0.48	0.44	0.07	0.26	0.67	4.48
Sb	0.62	0.09	0.38	0.53	0.07	0.13	0.80	0.53	0.30	0.04	0.70	0.26	0.05	0.37	0.58	3.06
Sc	0.65	0.10	0.35	0.55	0.08	0.08	0.84	0.53	0.14	0.02	0.86	0.12	0.04	0.51	0.45	1.86
Sd	0.56	0.08	0.44	0.48	0.08	0.09	0.83	0.47	0.04	0.01	0.96	0.03	0.02	0.77	0.21	1.05
Im	0.00	0.00	1.00	0.00	0.00	1.00	0.00	0.07	0.00	0.00	1.00	0.00	0.00	1.00	0.00	0.66
	[Fe/H][e]$_{tot}$	Disc colours $(U-V)$	$(B-V)$	$(V-K)$	Integrated colours $(U-V)$	$(B-V)$	$(V-K)$		[Fe/H]$_{tot}$	Disc colours $(U-V)$	$(B-V)$	$(V-K)$	Integrated colours $(U-V)$	$(B-V)$	$(V-K)$	
E	+0.00				0.74	0.66	2.82		+0.00				1.38	0.92	3.22	
S0	−0.09	0.60	0.60	2.55	0.71	0.64	2.77		−0.09	1.18	0.87	2.96	1.33	0.91	3.17	
Sa	−0.17	0.20	0.43	2.34	0.53	0.58	2.68		−0.24	0.60	0.63	2.70	0.91	0.76	2.98	
Sb	−0.19	0.10	0.38	2.27	0.47	0.55	2.66		−0.34	0.44	0.56	2.59	0.63	0.65	2.81	
Sc	−0.18	0.01	0.34	2.20	0.45	0.55	2.66		−0.43	0.34	0.51	2.51	0.43	0.56	2.63	
Sd	−0.21	−0.04	0.32	2.16	0.36	0.51	2.60		−0.49	0.28	0.48	2.46	0.31	0.49	2.50	
Im	−0.50	−0.07	0.30	2.13	−0.07	0.30	2.13		−0.50	0.24	0.46	2.42	0.24	0.46	2.42	

[a]Bulge+ halo luminosity fraction in bolometric. [b]Luminosity partition in bolometric. [c]Mass partition of the stellar component. [d]Stellar mass-to-light ratio of the model, in bolometric and solar units. [e]Luminosity-weighted mean metallicity of the model from the bolometric, defined as $\mathrm{Fe/H}]_{tot} = \sum_j [\mathrm{Fe/H}]_j (L_j/L_{tot})$, with $j = 1, 2, 3$ for the three galaxy components (i.e. halo, disc and bulge). The adopted value of $[\mathrm{Fe/H}]_j$ for each component is from Table 2.

© Royal Astronomical Society • Provided by the NASA Astrophysics Data System

2005MNRAS.361..725B

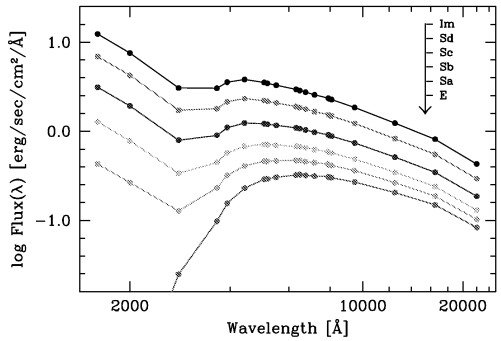

Figure 6. Theoretical SED for 15-Gyr template models of $M_{\rm gal} = 10^{11}\,{\rm M}_{\odot}$ along the Hubble sequence. Multicolour magnitudes have been converted to monocromatic flux density according to the photometric zero-points of Table 1. The ultraviolet flux estimates at 1600, 2000, and 2800 Å are from Paper I.

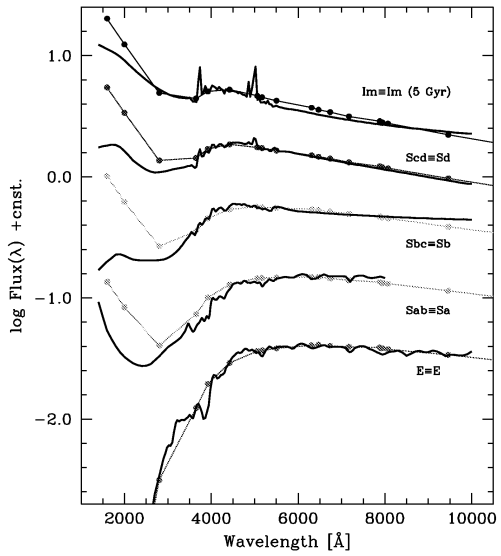

Figure 7. The SED for template galaxy models (connected solid dots) is compared with 'mean' empirical spectra along the Hubble morphological sequence (thick solid line). Data for types E (the M81 case), Sbc, Scd, and Im are from Coleman et al. (1980), while the Sab case is from Pence (1976). Empirical and theoretical templates are matched as labelled on each plot.

approach is allowed for composite stellar populations. From equation (2), at 15 Gyr we have that $\mathrm{SFR}_{\rm o} = b\,\langle\,\mathrm{SFR}\rangle = b\,\mathrm{M}_{\rm disc}/(15\times 10^9\ \mathrm{yr})$, and the current SN+HN event rate, $R_{\rm SN+HN} = \mathrm{d}\,N_{\rm SN+HN}/\mathrm{d}\,t$, can therefore be written as

$$R_{\rm SN+HN} = 0.0142\,\mathrm{SFR}_{\rm o} = 0.0142\,b\,f\,\frac{M_{\rm gal}}{(15\times 10^9\ \mathrm{yr})}, \qquad (9)$$

f being the stellar mass fraction of the disc (see Table 3). We could more suitably arrange equation (9) in terms of the bolometric mass-to-light ratio and total B luminosity of the parent galaxy (again, see Table 3 for the reference quantities). With a little arithmetic, $R_{\rm SN+HN}$ eventually becomes

$$R_{\rm SN+HN} = 0.95\,b\,f\left(\frac{M}{L_{\rm bol}}\right)10^{-0.4({\rm Bol}-B+0.69)}\,L^{B}_{10}. \qquad (10)$$

In this equation, L^{B}_{10} is the galaxy B-luminosity in units of $10^{10}\,\mathrm{L}^{B}_{\odot}$, while (Bol − B) is the galaxy bolometric correction to the Johnson B-band, derived from Tables A3–A7 as (Bol − B) = (Bol − V) − (B − V). With this notation, equation (10) directly provides the SN+HN rate in the usual SNu units [i.e. 1 SNu = 1 SN(100 yr)$^{-1}$(10^{10} L$^{B}_{\odot}$)$^{-1}$].

Table 4. Theoretical SN (II+Ibc) and hypernova rates for late-type galaxies at present time.

Hubble type	SN+HN$^{(a)}$ [SNu]	HN$^{(a)}$ [SNu]	$\tau^{(b)}_{\rm SN+HN}$ [yr]	$\tau^{(b)}_{\rm HN}$ [yr]
Sa	0.52	0.025	194	4100
Sb	1.10	0.052	91	1900
Sc	1.50	0.071	67	1400
Sd	1.74	0.082	58	1250
Im	1.91	0.090	52	1100

^{a}SN(II+Ibc)+HN and HN rates, in SNu units.
^{b}Expected times-cale between two SN or HN events in a 10^{11}-M$_{\odot}$ galaxy.

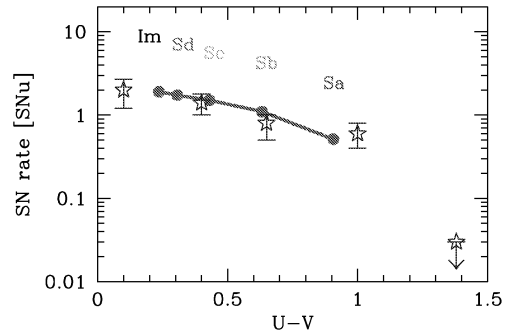

Figure 8. Theoretical SN(II+Ibc) rates, singled out from equations (10) and (8) (solid line and dots), are compared with the empirical estimates of Cappellaro et al. (1999) (star markers) from their survey of over 10 000 low-redshift galaxies. The $U-V$ refers to the galaxy integrated colour (corrected for reddening in case of observations).

Table 4 summarizes our results for late-type galaxies. In addition to the theoretical event rate, we also report in the table the typical time-scale elapsed between two SN and HN bursts in a 10^{11}-M$_{\odot}$ galaxy. As $R_{\rm SN+HN}$ tightly depends on SFR, it should correlate with galaxy ultraviolet colours; this is shown in Fig. 8, where a nice agreement is found with the empirical SN rates from the recent low-redshift galaxy survey by Cappellaro, Evans & Turatto (1999).

4.2 Back-in-time evolution

Theoretical luminosity evolution for disc-dominated systems in the Johnson U-, V-, K-bands, and for the bolometric, is displayed in the upper panels of Fig. 9; to each plot we also added a shaded curve that traces the value of $M_{\rm gal}$ versus time. The lower panels in the figure represent the expected evolution of the morphological parameter S/T for the same photometric bands. One striking feature in the Sa–Sd plots is the increasing luminosity contribution of the bulge at early epochs ($L_{\rm bulge}\propto t^{-0.8}$ in bolometric, see Table 1). This greatly compensates the drop in disc luminosity ($L_{\rm disc}\propto t\,L_{\rm bulge}$, from equation 1, for a constant SFR), and acts in the sense of predicting more nucleated (S/T → 1) galaxies at high redshift compared with present-day (i.e. 15 Gyr) objects.

This effect is shown in Fig. 10, where we track back-in-time evolution of the morphology parameter S/T in the ultraviolet range (Johnson U-band). Due to bulge enhancement, one sees that later-type spirals (Sc–Sd types) at 1 Gyr closely resemble present-day S0–Sa systems.

© Royal Astronomical Society • Provided by the NASA Astrophysics Data System

2005MNRAS.361..725B

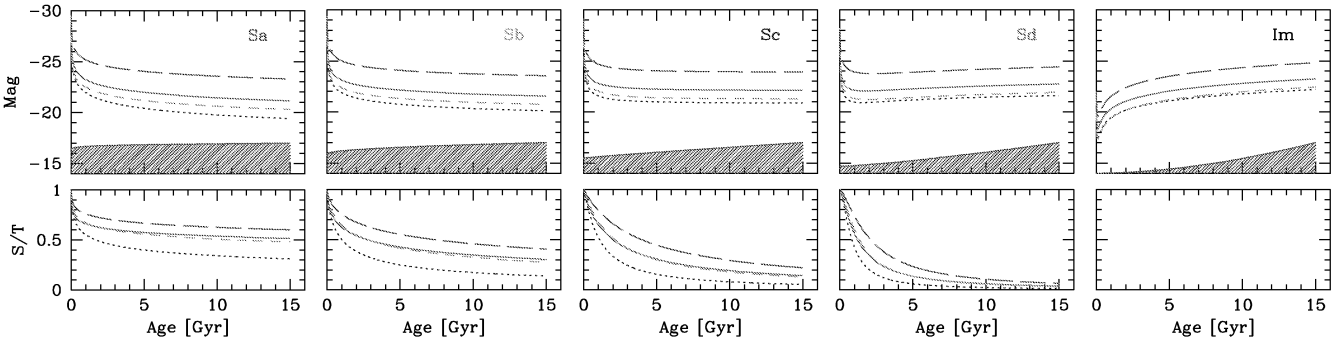

Figure 9. *Upper plots in each panel:* theoretical luminosity evolution for late-type galaxy models. A total stellar mass $M_{\rm gal} = 10^{11}\,{\rm M}_{\odot}$ is assumed at 15 Gyr. Solid lines track bolometric magnitude, while dotted lines are for the U-band, short-dashed for V-band, and long-dashed for the K-band. The shaded area in each plot sketches (on an arbitrary linear scale) the evolution of $M_{\rm gal}$ according to star formation history for each morphological type. *Lower plots in each panel:* the corresponding evolution of the morphological parameter S/T in the bolometric, U-, V- and K bands (same line caption as in the upper panels). Note that S/T $\rightarrow$ 1 at early epochs (excepting the Im model) due to the increasing bulge contribution.

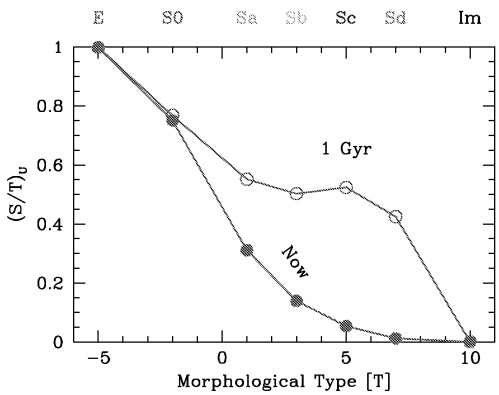

Figure 10. Inferred evolution of the U-band morphological parameter S/T for galaxies along the Hubble sequence. Bulge enhancement at early epochs leads later-type systems (Sc-Sd types) at 1 Gyr to closely resemble present-day S0-Sa galaxies.

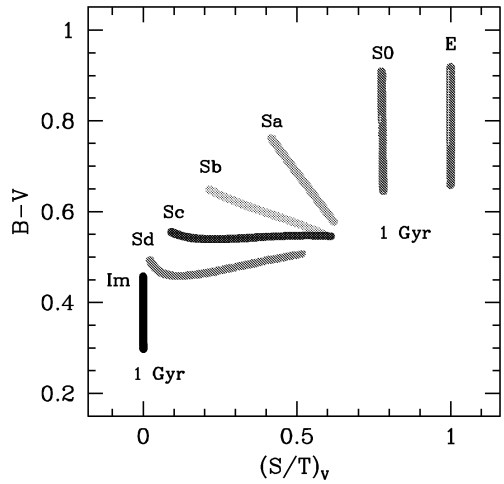

Figure 11. Rest-frame $B - V$ colour evolution, from 15 to 1 Gyr, versus V-band morphological parameter S/T for galaxy models along the Hubble sequence. The increasing luminosity contribution of the bulge component back in time makes spiral galaxies at high redshift more nucleated than present-day homologues. For high-redshift observations this induces a bias toward both 'spiked' and irregular systems with increasing distances (consider the x-axis projection of the figure) and conspires against the detection of grand-design spirals.

A colour versus S/T plot, like in Fig. 11, effectively summarizes overall galaxy properties at the different ages. Colour evolution is much shallower for spirals than for ellipticals and, as expected, the trend is always in the sense of having bluer galaxies at earlier epochs (excepting perhaps Sd spirals) independently of the star formation details. Rest-frame colours tend however to 'degenerate' with primeval late-type galaxies approaching the E model at early epochs as a consequence of the bulge brightening.

If one does not mind evolution, all these effects could lead to a strongly biased interpretation of high-redshift observations. For example, by relying on the apparent colours of the galaxy (that is by reading Fig. 11 from the y-axis, with no hints about morphology), the high-redshift galaxy population might show a lack of (intrinsically) red objects (ellipticals?), and enhance, on the contrary, blue galaxies (spirals?). On the other hand, if we account for apparent morphology alone (that is by reading Fig. 11 from the x-axis), then a bimodal excess of bulge-dominated systems (S/T $\rightarrow$ 1) and irregular star-forming galaxies (S/T $\sim$ 0) would appear at large distances (van den Bergh et al. 2000; Kajisawa & Yamada 2001). In fact, fiducial Im systems would eventually dominate with increasing redshift due to the disfavouring effect of k-correction on ellipticals, at least in the optical range. Among others, this should also conspire against the detection of grand-design spirals in high-redshift surveys (e.g. van den Bergh et al. 1996).

4.3 Redshift and age bias

The effect of redshift, and its induced selective sampling of galaxy stellar population with changing wavelength, has even more pervasive consequences, as we track the evolution of star-forming systems at increasing distances.

According to equation (1), the mean luminosity-weighted age of stars contributing to galaxy luminosity can be written as

$$\overline{t}_{*} = \frac{\int_0^t \tau\, L_{\rm SSP}(\tau){\rm SFR}(t-\tau)\,{\rm d}\tau}{L_{\rm tot}(t)}. \qquad (11)$$

The 'representative' age of stars changes therefore across the SED of the galaxy, since $L_{\rm SSP} \propto t^{-\alpha}$, and α depends on wavelength (cf. Table 1). As, in our parametrization, SFR $\propto t^{-\eta}$, then equation (11)

© Royal Astronomical Society • Provided by the NASA Astrophysics Data System

2005MNRAS.361..725B

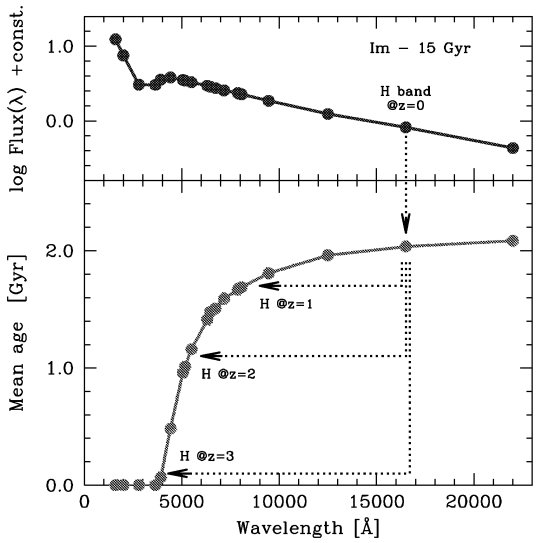

Figure 12. Theoretical SED for the 15-Gyr Im galaxy model (*upper panel*), and 'mean' age, $\bar{t}_*$, of the prevailing stars in the different photometric bands, according to equation (12) (*lower panel*). Note that younger (and more massive) stars contribute, on average, to global luminosity at shorter wavelength. Assuming we observe this galaxy in the infrared H-band at increasing distances (namely, from $z = 0$ to 3, as labelled), one might notice an apparent increase in the fresh star-formation activity with redshift (and a correspondingly younger inferred age) just as a consequence of probing blue/ultraviolet emission in the galaxy rest-frame.

becomes

$$\bar{t}_* = \frac{\int_0^t \tau^{1-\alpha}\,(t-\tau)^{-\eta}\,\mathrm{d}\tau}{\int_0^t \tau^{-\alpha}\,(t-\tau)^{-\eta}\,\mathrm{d}\tau} = \frac{1-\alpha}{2-\alpha-\eta}\,t. \qquad (12)$$

In bolometric, $\alpha \simeq 0.8$, that is, for a constant SFR, $\bar{t}_* \simeq 0.2\,t$; at 15 Gyr, bright stars are therefore on average ∼3 Gyr old. As an instructive example, in Fig. 12 we displayed the mean age of stars contributing to galaxy luminosity at different wavelengths for our 15-Gyr Im template model. Note that the value of $\bar{t}_*$ smoothly decreases at shorter wavelength, reaching a cut-off about 4000 Å, when α exceeds unity and $\bar{t}_*$ coincides with the lifetime of the highest mass stars in the IMF (see Paper I for the important consequences of this feature on galaxy ultraviolet SED). As a consequence, when tracking redshift evolution of star-forming galaxies through a given optical/infrared photometric band, one would be left with the tricky effect that distant objects appear to be younger than local homologues *in spite of any intrinsic evolution*.

5 LUMINOSITY CONTRIBUTION FROM RESIDUAL GAS

In addition to the prevailing role of stars, a small fraction of the luminosity of the galaxy (especially in late-type systems) is provided also by residual gas. Its contribution is both in terms of continuum emission, mainly from free–bound e^- transitions in the H II regions, and emission-line enhancement. This is the typical case of the Balmer series, for instance, but also some forbidden lines, like those of [O II] at 3727 Å and [O III] at 5007 Å, usually appear as a striking feature in the galactic spectrum (Kennicutt 1992; Sodré & Stasińska 1999).

The key triggering process for gas luminosity is the ultraviolet emission from short-living ($t \lesssim 10^7$ yr) stars of high mass ($M_* \gtrsim 10\,\mathrm{M}_\odot$), that supply most of the ionizing Lyman photons in the H II regions. The presence of emission lines is, in this sense, the most direct probe of ongoing star formation in a galaxy. If gas is optically thin and tracks the distribution of young stars, then one could expect a tight relationship between the actual SFR (via the number of UV-emitting stars) and the strength of the hydrogen emission lines.

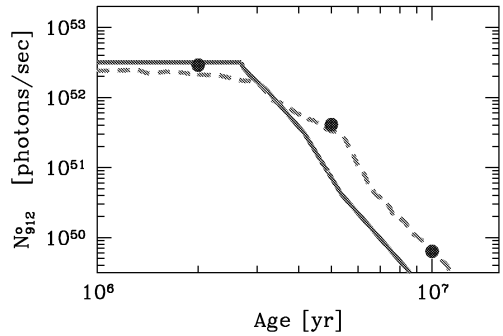

Figure 13. The expected rate of Lyman photons, N°_{912}, for a Salpeter SSP of $10^6\,\mathrm{M}_\odot$ with stars in the range 0.1–120 $\mathrm{M}_\odot$. Our results (thick solid line) consistently compare with the starburst models of Leitherer et al. (1999) (dashed line), and Mas-Hesse & Kunth (1991) (solid dots). Both these models have been rescaled to our output by matching the number of stars between 60 and 100 $\mathrm{M}_\odot$.

For its complexity, a detailed treatment of the nebular emission is obviously beyond the scope of this paper (see, e.g. Stasińka 2000 and Magris, Binette & Bruzual 2003, for a reference discussion on this subject). Here, we are rather interested in exploring the general trend of some relevant features, like the Balmer emission lines, that could supply an effective tool for SFR diagnostics when compared with observations.

5.1 Nebular emission

Our approach is similar to that of Leitherer & Heckman (1995), adopting for the gas, standard physical conditions, with $T = 10\,000$ K and $Y = 0.28$ for helium abundance (in mass). We will assume a full opacity to Lyman photons so that, once the photon rate N°_{912} from high-mass stars can be set from the detailed synthesis model, the nebular continuum is

$$L_{\mathrm{gas}}(\lambda) = \frac{c}{\lambda^2}\frac{\gamma_\lambda}{\alpha_B}N^{\circ}_{912}. \qquad (13)$$

In the equation, $\gamma(\lambda)$ is the continuum emission coefficient for the H–He chemical mix, according to Aller (1984), and includes both free–free and bound–free transitions by hydrogen and neutral helium, as well as the two-photon continuum of hydrogen. The hydrogen recombination coefficient (according to Case B of Baker & Menzel 1938) is from Osterbrok (1974) and has been set to $\alpha_B = 2.59\ 10^{-13}\,\mathrm{cm}^3\,\mathrm{s}^{-1}$.

According to equation (13), the nebular continuum directly scales with N°_{912} so that, as a relevant output of our models, in Fig. 13 we compute the expected rate of $\lambda < 912$ Å photons for a Salpeter SSP with upper cut-off mass at 120 $\mathrm{M}_\odot$. Our results compare consistently with the starburst models of Leitherer et al. (1999), and Mas-Hesse & Kunth (1991). To account for different IMF slope and/or stellar mass limits, comparison is made by matching our number of stars between 60 and 100 $\mathrm{M}_\odot$ in a $10^6\,\mathrm{M}_\odot$ SSP. The agreement between the models is fairly good, with a tendency for our SSP, however, to evolve faster given a slightly shorter lifetime assumed for high-mass stars (cf. Paper I for more details on the adopted stellar clock).

© Royal Astronomical Society • Provided by the NASA Astrophysics Data System

2005MNRAS.361..725B

5.2 Balmer emission-line evolution

The equivalent width of Balmer lines has been derived via the Hβ luminosity, defined as

$$L(\mathrm{H}\beta) = h\nu_{\mathrm{H}\beta}\,\frac{\alpha_{\mathrm{H}\beta}}{\alpha_B}\,N^{\mathrm{o}}_{912}. \qquad (14)$$

For the effective recombination coefficient at $T = 10\,000$ K we adopted the value $\alpha_{\mathrm{H}\beta} = 3.03 \times 10^{-14}\,\mathrm{cm^3\,s^{-1}}$ from Osterbrok (1974). This eventually leads to a calibration for the Hβ luminosity such as

$$L(\mathrm{H}\beta) = 4.78 \times 10^{-13}\,N^{\mathrm{o}}_{912}\,[\mathrm{ergs^{-1}}]. \qquad (15)$$

This result agrees within 0.4 per cent both with the Leitherer & Heckman (1995) and Copetti, Pastoriza & Dottori (1986) calculations. Balmer-line intensities, relative to Hβ, are from Osterbrok (1974, table 4.2 therein) for the relevant value of the temperature.

If the continuum (including both the contribution from stars and gas, L_* and L_{gas}, respectively) is assumed to vary slowly with wavelength, adjacent to the line, then the Hβ equivalent width can be written as

$$W(\mathrm{H}\beta) = \frac{L(\mathrm{H}\beta)}{(L_* + L_{\mathrm{gas}})} \qquad (16)$$

and all the other lines derive accordingly. The computed value of $W(\mathrm{H}\beta)$ should be regarded of course as the *net* emission from the gas component (that is after correcting the spectral feature for stellar absorption).

In Table 5 we report our final results, also summarized in Fig. 14. The upper panel of the figure displays the Balmer-line evolution for each of our template galaxies. As expected, Hα is the dominating feature, while gas emission noticeably decreases for Hγ and Hδ. In addition, the onset of the galaxy bulge at early epochs works in the sense of decreasing line emission because of the 'diluting' factor L_* in equation (16) (cf. for example the diverging path of Im and Sd evolution in Fig. 14).

In the lower panel of the same figure we computed the fraction $L_{\mathrm{gas}}/(L_* + L_{\mathrm{gas}})$ supplied by the nebular emission to the galaxy continuum at different wavelengths, between 4100 and 6600 Å, evaluated close to each Balmer line. As far as the galaxy broad-band colours are concerned, we see that nebular luminosity is almost negligible in our age range, and contributes at most a few per cent to the total luminosity of the galaxy.

One striking feature that stems from the analysis of Fig. 14 is the relative insensitivity of Balmer-line equivalent width to time. This is a consequence of the birth-rate law assumed in our models. Actually, for the case of Hβ, like in equation (16) for instance, we have that $L(\mathrm{H}\,\beta)$ mainly responds to $\mathrm{SFR_o}$, through the selective contribution of hot stars of high mass, while the contiguous spectral continuum collects a much more composite piece of information from all stars (and it is, roughly, $L_* \propto \langle\,\mathrm{SFR}\rangle$); this makes $W(\mathrm{H}\beta)$ better related to b. In our framework, we could therefore conclude that observation of Balmer emissions certainly provides important clues to size up the actual star formation activity in a galaxy, but it will barely constrain age.

6 SUMMARY AND CONCLUSIONS

In this work we attempted a comprehensive analysis of some relevant aspects of galactic photometric evolution. Colours and basic morphological features for early- and late-type systems have been reproduced by means of a set of theoretical population synthesis models, which evaluate the individual photometric contribution of the three main stellar components of a galaxy, namely the bulge, disc and halo.

Table 5. Balmer-line intensities for late-type galaxy templates. The listed quantity is the Balmer emission-line equivalent width in Å.

Age	Sa				Sb				Sc			
[Gyr]	Hδ	Hγ	Hβ	Hα	Hδ	Hγ	Hβ	Hα	Hδ	Hγ	Hβ	Hα
1.0	0.55	1.63	4.11	13.8	0.79	2.33	6.01	20.6	0.88	2.59	6.73	23.1
1.5	0.56	1.63	4.05	13.3	0.84	2.49	6.35	21.4	1.03	3.02	7.86	26.9
2.0	0.56	1.64	4.00	13.0	0.88	2.58	6.55	21.9	1.12	3.29	8.56	29.3
3.0	0.56	1.64	3.93	12.4	0.91	2.69	6.76	22.3	1.22	3.58	9.36	32.1
4.0	0.56	1.64	3.87	12.1	0.93	2.75	6.87	22.5	1.27	3.73	9.76	33.5
5.0	0.56	1.64	3.83	11.8	0.95	2.79	6.92	22.5	1.29	3.80	9.97	34.2
6.0	0.56	1.64	3.79	11.6	0.95	2.81	6.95	22.5	1.31	3.84	10.1	34.5
8.0	0.55	1.63	3.73	11.2	0.96	2.83	6.96	22.3	1.31	3.87	10.1	34.6
10.0	0.55	1.63	3.68	10.9	0.97	2.84	6.95	22.1	1.31	3.86	10.1	34.3
12.5	0.55	1.62	3.62	10.6	0.97	2.85	6.92	21.9	1.30	3.84	9.98	33.9
15.0	0.55	1.62	3.58	10.4	0.97	2.84	6.88	21.6	1.29	3.80	9.85	33.3

Age	Sd				Im			
[Gyr]	Hδ	Hγ	Hβ	Hα	Hδ	Hγ	Hβ	Hα
1.0	1.20	3.54	9.46	33.4	2.62	7.71	24.0	99.9
1.5	1.43	4.20	11.4	40.7	2.42	7.13	21.9	90.1
2.0	1.54	4.54	12.5	45.0	2.29	6.76	20.5	83.2
3.0	1.63	4.81	13.3	48.6	2.13	6.28	18.7	74.6
4.0	1.65	4.87	13.5	49.5	2.03	5.98	17.6	69.2
5.0	1.65	4.86	13.5	49.4	1.95	5.76	16.8	65.3
6.0	1.64	4.82	13.4	48.8	1.90	5.59	16.2	62.3
8.0	1.60	4.72	13.0	47.4	1.81	5.34	15.3	57.9
10.0	1.57	4.64	12.7	45.9	1.75	5.15	14.6	54.6
12.5	1.54	4.52	12.3	44.2	1.69	4.97	14.0	51.6
15.0	1.50	4.43	12.0	42.7	1.64	4.84	13.5	49.4

© Royal Astronomical Society • Provided by the NASA Astrophysics Data System

2005MNRAS.361..725B

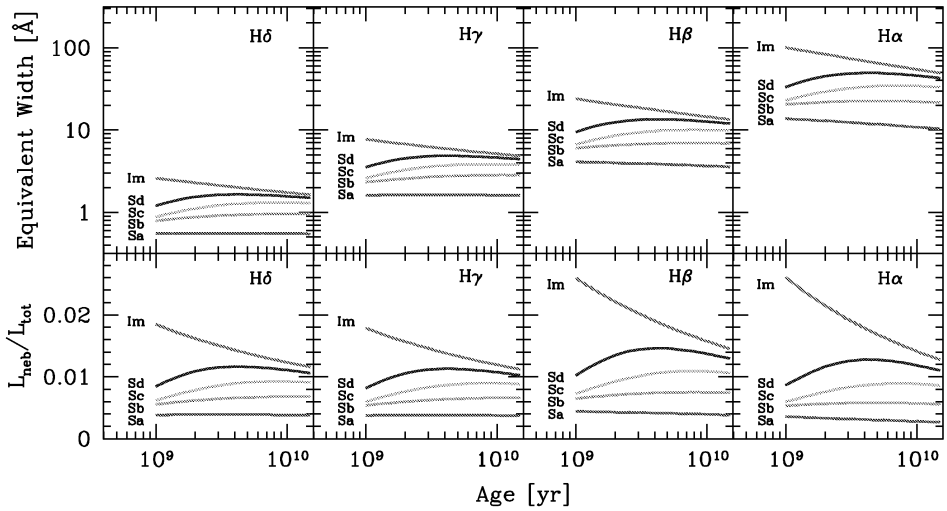

Figure 14. Expected evolution for Balmer emission and nebular luminosity from residual gas in our late-type galaxy templates. Upper panel displays the equivalent width of each Balmer feature with galaxy age. The lower panel is the fraction of nebular luminosity supplied to the total galaxy continuum evaluated at the relevant wavelength close to each Balmer line.

Facing the formidable complexity of the problem (and the lack, to our present knowledge, of any straightforward 'prime principle' governing galactic evolution), we chose to adopt a 'heuristic' point of view, where the distinctive properties of present-day galaxies derive from a minimal set of physical assumptions and are mainly constrained by the observed colours along the Hubble sequence.

One important feature of our models is that the galactic SFR is a natural output of the gas-to-star conversion efficiency, which we assume to be an intrinsic and distinctive feature of the morphological type of the galaxy (see equation 2). Our treatment of the star versus gas interplay is therefore somewhat different from other popular approaches, that rely on the Schmidt law.[7]

Our results show that star formation history, as a function of the overall disc composition along the late-type galaxy sequence, appears to be a main factor in modulating the photometric properties of the galaxy. In general, the disc photometric contribution is the prevailing one in the luminosity (but not necessarily in the mass) budget of present-day galaxies. Table 3 shows, for instance, that less than a half of the total mass of a Sbc galaxy like the Milky Way is stored in the disc stars, while the latter provide over 3/4 of the global luminosity.

As shown in Fig. 4, the observed colours of present-day galaxies tightly constrain the stellar birth rate, leading to a smooth increasing trend for b from E to Im types (cf. Table 2 and also fig. 8 in Paper I).

The comparison with observed SN rate is an immediate 'acid test' for our models, due to the marked sensitivity of this parameter to the current SFR. The remarkably tuned match of our theoretical output with the SN observations in low-redshift galaxies (cf. Fig. 8) is, in this regard, extremely encouraging. As a possibly interesting feature for future observational feedback, we give in Table 4 also a prediction of the hypernova event rate in late-type galaxies; this quite new class of stars is raising increasing interest for its claimed relationship with gamma-ray bursts and the possible relevant impact of these events on cosmological studies.

Another important point of our theoretical framework deals with the fact that galaxy evolution is tracked in terms of the individual history of the different galaxy subsystems. This is a non-negligible aspect, as diverging evolutionary paths are envisaged for the bulge versus disc stellar populations. As discussed in Section 4.2, one has to expect that $L_{\rm bulge}/L_{\rm disc} \propto t^{-1}$, that is the bulge always ends up as the dominant contributor to galaxy luminosity at early epochs.

As a consequence, the current morphological appearance of galaxies might drastically change when moving to larger distances, and we have shown in Section 4 how this bias could affect the observation (and the interpretation) of high-redshift surveys.

In addition to broad-band colours, we have also briefly assessed the photometric contribution of the nebular gas, studying in particular the expected evolution of Balmer line emission in disc-dominated systems. As a main point in our analysis, models show that striking emission lines, like Hα, can very effectively track stellar birth rate in a galaxy. For these features to be useful age tracers as well, however, one should first assess how b could really change with time on the basis of supplementary (and physically independent) arguments.

As a further follow-up of this work, we finally plan to complete the analysis of these galaxy template models providing, in a future paper, also the evolutionary k-corrections and other reference quantities for a wider application of the model output to high-redshift studies.

[7] After all, even the Schmidt law is nothing more that one 'reasonable' (but none the less arbitrary) assumption in the current theory of late-type galaxy evolution. In this respect, for instance, there has been growing evidence that a classical dependence such as $\dot{M}_* \propto \rho_{\rm gas}^n$ (whatever the value for n) is to some extent inadequate for a general description of the SFR (Talbot & Arnett 1975; Larson 1976; Dopita 1985; Silk 1988; Wyse & Silk 1989; Ryder & Dopita 1994).

ACKNOWLEDGMENTS

I wish to dedicate this work to my baby, Valentina, and to her mom Claribel, for their infinite patience and invaluable support during the three years spent on this project.

REFERENCES

Aaronson M., 1978, ApJ, 221, L103
Aller L. H., 1984, Physics of Thermal Gaseous Nebulae. Reidel, Dordrecht

© Royal Astronomical Society • Provided by the NASA Astrophysics Data System

2005MNRAS.361..725B

Arimoto N., Jablonka P., 1991, A&A, 249, 374
Arimoto N., Yoshii Y., 1986, A&A, 164, 260
Baker J. G., Menzel D. H., 1938, ApJ, 88, 52
Bessell M. S., 1979, PASP, 91, 589
Bressan A., Chiosi C., Fagotto F., 1994, ApJS, 94, 63
Brodie J. P., Huchra J. P., 1991, ApJ, 379, 157
Bruzual A. G., Charlot S., 2003, MNRAS, 344, 1000
Bruzual A. G., Kron R. G., 1980, ApJ, 241, 25
Bruzual A. G., Magris G. C., Calvet N., 1988, ApJ, 333, 673
Buta R., Mitra S., de Vaucouleurs G., Corwin H. G. Jr, 1994, AJ, 107, 118
Buzzoni A., 1989, ApJS, 71, 817
Buzzoni A., 1995, ApJS, 98, 69
Buzzoni A., 2002, AJ, 123, 1188 (Paper I)
Buzzoni A., Arnaboldi M., Corradi R. L. M. 2005, MNRAS, submitted
Calzetti D., 1999, Mem. Soc. Astr. It., 70, 715
Canterna R., 1976, AJ, 81, 228
Cappellaro E., Evans R., Turatto M., 1999, A&A, 351, 459
Cellone S. A., Forte J. C., 1996, ApJ, 461, 176
Cerviño M., Valls-Gabaud D., 2003, MNRAS, 338, 481
Cerviño M., Valls-Gabaud D., Luridiana V., Mas-Hesse J. M., 2002, A&A, 381, 51
Charlot S., Worthey G., Bressan A., 1996, ApJ, 457, 625
Coleman C. D., Wu C. C., Weedman D. W., 1980, ApJS, 43, 393
Copetti M. V. F., Pastoriza M. G., Dottori H. A., 1986, A&A, 156, 111
Davidge T. J., 2001, AJ, 122, 1386
de Jong R. S., 1996, A&A, 313, 45
de Loore C., 1988, A&A, 203, 71
de Vaucouleurs G., de Vaucouleurs A., Corwin H. G. Jr, Buta R. J., Paturel G., Fouque P., 1991, Third Reference Catalog of Bright Galaxies. Springer, Heidelberg
Dopita M. A., 1985, ApJ, 295, 5
Durrell P. R., Harris W. E., Geisler D., Pudritz R. E., 1996, AJ, 112, 972
Dwek E. et al., 1995, ApJ, 445, 716
Edvardsson B., Andersen J., Gustaffson B., Lambert D. L., Nissen P. E., Tomkin J., 1993, A&A, 275, 101
Feltzing S., Gilmore G., 2000, A&A, 355, 949
Firmani C., Tutukov A. V., 1992, A&A, 264, 37
Firmani C., Tutukov A. V., 1994, A&A, 288, 713
Frogel J. A., 1988, ARA&A, 26, 51
Frogel J. A., 1999, Ap&SS, 265, 303
Fukugita M., Shimasaku K., Ichikawa T., 1995, PASP, 107, 945
Fukugita M., Ichikawa T., Gunn J. E., Doi M., Shimasaku K., Schneider D. P., 1996, AJ, 111, 1748
Gavazzi G., 1993, ApJ, 419, 469
Gavazzi G., Scodeggio M., 1996, A&A, 312, 29
Gavazzi G., Boselli A., Kennicutt R., 1991, AJ, 101, 1207
Geisler D., Friel E. D., 1992, AJ, 104, 128
Gilmore G., King I., van der Kruit P., 1990, The Milky Way as a Galaxy. University Science Books, Mill Valley
Giovanardi C., Hunt L. K., 1988, AJ, 95, 408
Goudfrooij P., Gorgas J., Jablonka P., 1999, Ap&SS, 269, 109
Harris W. E., 1996, AJ, 112, 1487
Iwamoto K. et al., 1998, Nat, 395, 672
Jablonka P., Martin P., Arimoto N., 1996, in Buzzoni A., Renzini A., Serrano A., eds, ASP Conf. Ser., Vol. 86, Fresh Views of Elliptical Galaxies. Astron. Soc. Pac., San Francisco, p. 185
Kajisawa M., Yamada T., 2001, PASJ, 53, 833
Kent S. M., 1985, ApJS, 59, 115
Kennicutt R. C. Jr, 1992, ApJ, 388, 310
Kennicutt R. C. Jr, 1998, ARA&A, 36, 189
Kennicutt R. C. Jr, Tamblyn P., Congdon C. W., 1994, ApJ, 435, 22
Kissler-Patig M. et al., 2003, in Kissler-Patig M., ed., ESO Astrophys. Symp., Extragalactic Globular Cluster Systems. Springer, Heidelberg, p. 117
Köppen J., Arimoto N., 1990, A&A, 240, 22
Larson R. B., 1975, MNRAS, 173, 671
Larson R. B., 1976, MNRAS, 176, 31
Larson R. B., Tinsley B. M., 1978, ApJ, 219, 46
Leitherer C., Heckman T. M., 1995, ApJS, 96, 9
Leitherer C. et al., 1999, ApJS, 123, 3
Lilly S. J., Longair M. S., 1984, MNRAS, 211, 833
Maeder A., Conti P. S., 1994, ARA&A, 32, 227
Magris C. G., Binette L., Bruzual A. G., 2003, ApJS, 149, 313
Mas-Hesse J. M., Kunth D., 1991, A&AS, 88, 399
Massarotti M., Iovino A., Buzzoni A., 2001, A&A, 368, 74
Moriondo G., Giovanardi C., Hunt L. K., 1998, A&AS, 130, 81
Nakamura T., Nomoto K., Iwamoto K., Umeda H., Mazzali P. A., Danziger I. J., 2000, Mem. Soc. Astron. It., 71, 345
Origlia L., Rich R. M., 2005, in Käufl H. U., Siebenmorgen R., Moorwood A. eds, ESO Astrophys. Symp., High-resolution Infrared Spectroscopy in Astronomy. Springer, Heidelberg, in press
Osterbrok D. E., 1974, Astrophysics of Gaseous Nebulae and Active Galactic Nuclei. University Science Books, Mill Valley
Paczynski B., 1998, ApJ, 494, L45
Pardi M. C., Ferrini F., 1994, ApJ, 421, 491
Pence W., 1976, ApJ, 203, 39
Perrett K. M., Bridges T. J., Hanes D. A., Irwin M. J., Brodie J. P., Carter D., Huchra J. P., Watson F. G., 2002, AJ, 123, 2490
Quirk W. J., Tinsley B. M., 1973, ApJ, 179, 69
Renzini A., 1993, in DeJonghe H., Habing H. J., eds, IAU Symp. No. 153, Galactic Bulges. Kluwer, Dordrecht, p. 151
Renzini A., Buzzoni A., 1986, in Chiosi C., Renzini A., eds, Spectral Evolution of Galaxies. Reidel, Dordrecht, p. 195
Rich R. M., 1990, ApJ, 362, 604
Roberts M. S., Haynes M. P., 1994, ARA&A, 32, 115
Ryder S. D., Dopita M. A., 1994, ApJ, 430, 142
Sadler E. M., Rich R. M., Terndrup D. M., 1996, AJ, 112, 171
Salpeter E. E., 1955, ApJ, 121, 161
Sandage A., 1986, A&A, 161, 89
Sandage A., 1987, AJ, 93, 610
Sandage A., Fouts G., 1987, AJ, 93, 74
Schneider D. P., Gunn J. E., Hoessel J. G., 1983, ApJ, 264, 337
Searle L., Sargent W. L. W., Bagnuolo W. G., 1973, ApJ, 179, 427
Silk J., 1988 in Pudritz R. E., Fich M., Galactic and Extragalactic Star Formation, NATO Advanced Science Institutes (ASI) Series C, 232, p. 503
Simien F., de Vaucouleurs G., 1983, in Athanassoula E., ed., IAU Symp. No. 100. Internal Kinematics and Dynamics of Galaxies. Reidel, Dordrecht, p. 375
Simien F., de Vaucouleurs G., 1986, ApJ, 302, 564
Sodré L. Jr, Stasińska G., 1999, A&A, 345, 391
Spinrad H., Taylor B., 1971, ApJS, 22, 445
Stasińska G., 2000, New Astron. Rev., 44, 275
Sweigart A. V., Gross P. G., 1978, ApJS, 36, 405
Talbot R. J. Jr, Arnett W. D., 1975, ApJ, 197, 551
Thuan T. X., Gunn J. E., 1976, PASP, 88, 543
Tiede G. P., Frogel J. A., Terndrup D. M., 1995, AJ, 110, 2788
Tinsley B. M., 1980, Fund. Cosm. Phys., 5, 287
Tinsley B. M., Gunn J. E., 1978, ApJ, 203, 52
van den Bergh S., Abraham R. G., Ellis R. S., Tanvir N. R., Santiago B. X., Glazebrook K. G., 1996, AJ, 112, 359
van den Bergh S., Cohen J. G., Hogg D. W., Blandford R., 2000, AJ, 120, 2190
Whitford A. E., Rich R. M., 1983, ApJ, 274, 723
Woosley S. E., MacFayden A. I., 2000, Mem. Soc. Astron. It., 71, 357
Wyse R. F. G., Silk J., 1989, ApJ, 339, 700
Yoshii Y., Takahara F., 1988, ApJ, 326, 1
Zinn R., 1980, ApJS, 42, 19
Zoccali M. et al., 2003, A&A, 399, 931

APPENDIX A: SYNTHETIC PHOTOMETRY FOR TEMPLATE GALAXY MODELS

We report, in the series of Tables A1–A7, the detailed output of the template galaxy models for the different Hubble morphological

© Royal Astronomical Society • Provided by the NASA Astrophysics Data System

2005MNRAS.361..725B

Table A1. Template model for E galaxies.

		Johnson							
Age [Gyr]	Bol	Bol − V	$U-V$	$B-V$	$V-R$	$V-I$	$V-J$	$V-H$	$V-K$
1.0	−23.100	−0.722	0.740	0.656	0.698	1.301	1.916	2.630	2.821
1.5	−22.736	−0.745	0.840	0.696	0.725	1.343	1.968	2.688	2.882
2.0	−22.493	−0.764	0.907	0.723	0.744	1.371	2.004	2.727	2.923
3.0	−22.142	−0.792	1.003	0.763	0.771	1.413	2.055	2.783	2.983
4.0	−21.888	−0.814	1.073	0.791	0.791	1.443	2.093	2.824	3.027
5.0	−21.698	−0.832	1.125	0.813	0.806	1.465	2.121	2.855	3.059
6.0	−21.543	−0.847	1.168	0.830	0.818	1.484	2.144	2.880	3.086
8.0	−21.298	−0.870	1.235	0.858	0.837	1.513	2.181	2.920	3.128
10.0	−21.106	−0.890	1.287	0.880	0.852	1.536	2.209	2.952	3.162
12.5	−20.919	−0.909	1.338	0.902	0.867	1.559	2.237	2.983	3.194
15.0	−20.764	−0.925	1.381	0.919	0.879	1.577	2.260	3.008	3.221

	Cousins		Gunn			Washington			
Age [Gyr]	$V-R_C$	$V-I_C$	$g-V$	$g-r$	$g-i$	$C-M$	$M-V$	$M-T_1$	$M-T_2$
1.0	0.488	1.018	0.154	0.251	0.417	0.494	0.230	0.639	1.223
1.5	0.508	1.050	0.163	0.282	0.460	0.551	0.242	0.667	1.269
2.0	0.522	1.072	0.169	0.303	0.489	0.590	0.250	0.686	1.300
3.0	0.542	1.105	0.178	0.334	0.531	0.645	0.262	0.714	1.345
4.0	0.556	1.128	0.184	0.356	0.562	0.685	0.271	0.734	1.378
5.0	0.567	1.145	0.189	0.373	0.585	0.715	0.277	0.749	1.402
6.0	0.576	1.160	0.193	0.386	0.604	0.740	0.283	0.762	1.422
8.0	0.590	1.182	0.200	0.408	0.634	0.779	0.291	0.781	1.454
10.0	0.601	1.200	0.204	0.425	0.658	0.809	0.298	0.797	1.479
12.5	0.612	1.218	0.209	0.442	0.681	0.839	0.304	0.812	1.504
15.0	0.621	1.232	0.213	0.456	0.700	0.864	0.310	0.824	1.524

Table A2. Template model for S0 galaxies.

		Johnson							
Age [Gyr]	Bol	Bol − V	$U-V$	$B-V$	$V-R$	$V-I$	$V-J$	$V-H$	$V-K$
1.0	−23.146	−0.699	0.710	0.644	0.686	1.277	1.881	2.584	2.769
1.5	−22.782	−0.721	0.807	0.684	0.714	1.320	1.934	2.642	2.830
2.0	−22.539	−0.738	0.872	0.711	0.733	1.348	1.969	2.681	2.871
3.0	−22.188	−0.766	0.966	0.751	0.760	1.390	2.021	2.738	2.931
4.0	−21.934	−0.787	1.034	0.779	0.780	1.420	2.058	2.779	2.975
5.0	−21.744	−0.804	1.085	0.801	0.795	1.442	2.086	2.810	3.007
6.0	−21.589	−0.818	1.126	0.818	0.807	1.461	2.109	2.835	3.034
8.0	−21.344	−0.841	1.192	0.846	0.826	1.490	2.146	2.875	3.077
10.0	−21.152	−0.859	1.243	0.868	0.841	1.513	2.175	2.906	3.110
12.5	−20.964	−0.878	1.293	0.890	0.856	1.536	2.203	2.937	3.142
15.0	−20.809	−0.893	1.334	0.908	0.868	1.554	2.226	2.963	3.169

	Cousins		Gunn			Washington			
Age [Gyr]	$V-R_C$	$V-I_C$	$g-V$	$g-r$	$g-i$	$C-M$	$M-V$	$M-T_1$	$M-T_2$
1.0	0.480	1.000	0.152	0.239	0.398	0.471	0.226	0.629	1.204
1.5	0.500	1.033	0.161	0.270	0.441	0.526	0.239	0.657	1.250
2.0	0.514	1.055	0.167	0.291	0.470	0.564	0.247	0.676	1.281
3.0	0.534	1.087	0.176	0.322	0.513	0.618	0.259	0.704	1.326
4.0	0.548	1.110	0.182	0.344	0.543	0.657	0.268	0.724	1.359
5.0	0.559	1.128	0.187	0.361	0.567	0.686	0.274	0.740	1.383
6.0	0.568	1.142	0.191	0.375	0.586	0.711	0.279	0.752	1.403
8.0	0.582	1.165	0.197	0.397	0.616	0.749	0.288	0.772	1.435
10.0	0.593	1.182	0.202	0.414	0.639	0.778	0.295	0.787	1.460
12.5	0.604	1.200	0.207	0.430	0.662	0.808	0.301	0.802	1.485
15.0	0.613	1.214	0.211	0.444	0.682	0.832	0.307	0.815	1.505

© Royal Astronomical Society • Provided by the NASA Astrophysics Data System

2005MNRAS.361..725B

Table A3. Template model for Sa galaxies.

		Johnson							
Age [Gyr]	Bol	Bol − *V*	*U* − *V*	*B* − *V*	*V* − *R*	*V* − *I*	*V* − *J*	*V* − *H*	*V* − *K*
1.0	−23.221	−0.737	0.530	0.576	0.649	1.220	1.809	2.504	2.683
1.5	−22.895	−0.750	0.594	0.605	0.671	1.253	1.850	2.548	2.730
2.0	−22.678	−0.760	0.636	0.625	0.685	1.275	1.877	2.578	2.761
3.0	−22.365	−0.776	0.695	0.653	0.706	1.307	1.917	2.620	2.806
4.0	−22.140	−0.788	0.736	0.674	0.722	1.330	1.946	2.651	2.838
5.0	−21.972	−0.798	0.766	0.689	0.733	1.348	1.967	2.674	2.862
6.0	−21.835	−0.806	0.790	0.701	0.743	1.362	1.984	2.693	2.882
8.0	−21.620	−0.820	0.827	0.720	0.757	1.384	2.012	2.723	2.913
10.0	−21.452	−0.831	0.856	0.735	0.769	1.402	2.034	2.746	2.938
12.5	−21.288	−0.841	0.884	0.750	0.780	1.419	2.055	2.769	2.962
15.0	−21.153	−0.850	0.907	0.762	0.790	1.433	2.073	2.788	2.982

	Cousins		Gunn			Washington			
Age [Gyr]	$V-R_C$	$V-I_C$	*g* − *V*	*g* − *r*	*g* − *i*	*C* − *M*	*M* − *V*	$M-T_1$	$M-T_2$
1.0	0.451	0.954	0.138	0.194	0.338	0.365	0.208	0.588	1.139
1.5	0.467	0.979	0.145	0.219	0.372	0.402	0.217	0.610	1.175
2.0	0.478	0.996	0.150	0.235	0.394	0.427	0.224	0.624	1.199
3.0	0.493	1.021	0.157	0.259	0.427	0.462	0.233	0.646	1.234
4.0	0.505	1.038	0.161	0.276	0.451	0.486	0.239	0.661	1.259
5.0	0.513	1.052	0.165	0.289	0.468	0.503	0.244	0.672	1.278
6.0	0.520	1.062	0.168	0.299	0.483	0.518	0.248	0.682	1.293
8.0	0.530	1.080	0.173	0.315	0.506	0.541	0.254	0.696	1.317
10.0	0.539	1.093	0.176	0.328	0.523	0.558	0.259	0.708	1.336
12.5	0.547	1.106	0.180	0.341	0.541	0.575	0.264	0.719	1.355
15.0	0.554	1.117	0.183	0.351	0.555	0.588	0.268	0.728	1.370

Table A4. Template model for Sb galaxies.

		Johnson							
Age [Gyr]	Bol	Bol − *V*	*U* − *V*	*B* − *V*	*V* − *R*	*V* − *I*	*V* − *J*	*V* − *H*	*V* − *K*
1.0	−23.114	−0.757	0.467	0.551	0.635	1.199	1.784	2.477	2.655
1.5	−22.842	−0.770	0.501	0.568	0.649	1.221	1.810	2.504	2.683
2.0	−22.667	−0.778	0.521	0.579	0.658	1.234	1.826	2.520	2.700
3.0	−22.422	−0.790	0.546	0.594	0.671	1.252	1.848	2.542	2.722
4.0	−22.252	−0.797	0.562	0.604	0.679	1.265	1.863	2.557	2.737
5.0	−22.128	−0.802	0.573	0.611	0.686	1.274	1.874	2.568	2.749
6.0	−22.030	−0.806	0.583	0.617	0.691	1.282	1.883	2.577	2.758
8.0	−21.878	−0.812	0.597	0.627	0.699	1.294	1.897	2.592	2.772
10.0	−21.763	−0.817	0.609	0.634	0.706	1.303	1.908	2.603	2.784
12.5	−21.653	−0.821	0.621	0.642	0.713	1.313	1.920	2.615	2.796
15.0	−21.565	−0.824	0.632	0.649	0.718	1.321	1.929	2.624	2.806

	Cousins		Gunn			Washington			
Age [Gyr]	$V-R_C$	$V-I_C$	*g* − *V*	*g* − *r*	*g* − *i*	*C* − *M*	*M* − *V*	$M-T_1$	$M-T_2$
1.0	0.441	0.937	0.133	0.178	0.316	0.328	0.201	0.573	1.116
1.5	0.451	0.953	0.138	0.194	0.338	0.347	0.207	0.587	1.139
2.0	0.458	0.963	0.141	0.204	0.351	0.359	0.211	0.596	1.154
3.0	0.467	0.977	0.144	0.217	0.370	0.373	0.216	0.608	1.174
4.0	0.473	0.986	0.147	0.227	0.383	0.382	0.220	0.616	1.188
5.0	0.478	0.993	0.149	0.234	0.393	0.388	0.222	0.622	1.198
6.0	0.481	0.999	0.151	0.239	0.401	0.394	0.224	0.627	1.206
8.0	0.487	1.008	0.153	0.248	0.413	0.402	0.228	0.635	1.219
10.0	0.492	1.015	0.155	0.256	0.423	0.409	0.231	0.642	1.230
12.5	0.497	1.022	0.157	0.263	0.433	0.417	0.233	0.648	1.240
15.0	0.501	1.029	0.159	0.269	0.442	0.423	0.236	0.653	1.249

© Royal Astronomical Society • Provided by the NASA Astrophysics Data System

2005MNRAS.361..725B

Table A5. Template model for Sc galaxies.

		Johnson							
Age [Gyr]	Bol	Bol − V	$U-V$	$B-V$	$V-R$	$V-I$	$V-J$	$V-H$	$V-K$
1.0	−22.799	−0.770	0.453	0.546	0.633	1.199	1.786	2.480	2.659
1.5	−22.594	−0.788	0.449	0.547	0.638	1.204	1.791	2.484	2.662
2.0	−22.478	−0.798	0.441	0.546	0.639	1.205	1.790	2.481	2.658
3.0	−22.341	−0.808	0.425	0.543	0.639	1.203	1.786	2.473	2.648
4.0	−22.264	−0.812	0.416	0.541	0.639	1.201	1.782	2.466	2.639
5.0	−22.218	−0.813	0.411	0.540	0.639	1.200	1.779	2.461	2.633
6.0	−22.187	−0.813	0.409	0.540	0.639	1.200	1.778	2.458	2.629
8.0	−22.149	−0.813	0.410	0.542	0.641	1.202	1.778	2.456	2.626
10.0	−22.128	−0.812	0.415	0.546	0.644	1.205	1.781	2.457	2.626
12.5	−22.115	−0.811	0.422	0.550	0.648	1.209	1.785	2.460	2.628
15.0	−22.108	−0.810	0.430	0.555	0.651	1.214	1.791	2.465	2.633

	Cousins		Gunn			Washington			
Age [Gyr]	$V-R_C$	$V-I_C$	$g-V$	$g-r$	$g-i$	$C-M$	$M-V$	$M-T_1$	$M-T_2$
1.0	0.440	0.936	0.132	0.176	0.314	0.321	0.200	0.570	1.114
1.5	0.443	0.940	0.133	0.180	0.320	0.317	0.201	0.574	1.120
2.0	0.443	0.940	0.134	0.181	0.321	0.311	0.202	0.574	1.121
3.0	0.443	0.938	0.134	0.180	0.320	0.300	0.201	0.574	1.120
4.0	0.443	0.936	0.134	0.180	0.319	0.294	0.201	0.573	1.119
5.0	0.443	0.935	0.134	0.180	0.319	0.290	0.201	0.573	1.119
6.0	0.443	0.935	0.134	0.181	0.319	0.288	0.202	0.574	1.119
8.0	0.445	0.936	0.135	0.183	0.322	0.288	0.203	0.576	1.122
10.0	0.446	0.938	0.136	0.186	0.326	0.290	0.204	0.579	1.126
12.5	0.449	0.942	0.137	0.190	0.331	0.294	0.205	0.582	1.132
15.0	0.452	0.946	0.138	0.194	0.336	0.299	0.207	0.586	1.138

Table A6. Template model for Sd galaxies.

		Johnson							
Age [Gyr]	Bol	Bol − V	$U-V$	$B-V$	$V-R$	$V-I$	$V-J$	$V-H$	$V-K$
1.0	−22.117	−0.796	0.362	0.508	0.610	1.163	1.739	2.428	2.603
1.5	−22.050	−0.818	0.314	0.489	0.600	1.144	1.713	2.395	2.566
2.0	−22.049	−0.826	0.283	0.476	0.591	1.129	1.692	2.368	2.536
3.0	−22.105	−0.829	0.252	0.463	0.582	1.110	1.665	2.332	2.496
4.0	−22.180	−0.827	0.242	0.459	0.578	1.103	1.652	2.315	2.475
5.0	−22.252	−0.823	0.242	0.459	0.578	1.101	1.648	2.308	2.466
6.0	−22.319	−0.820	0.246	0.462	0.579	1.102	1.648	2.306	2.463
8.0	−22.436	−0.814	0.259	0.468	0.584	1.107	1.653	2.309	2.465
10.0	−22.536	−0.810	0.273	0.476	0.589	1.115	1.661	2.317	2.473
12.5	−22.640	−0.806	0.290	0.485	0.596	1.124	1.673	2.329	2.485
15.0	−22.728	−0.804	0.306	0.493	0.602	1.134	1.684	2.341	2.497

	Cousins		Gunn			Washington			
Age [Gyr]	$V-R_C$	$V-I_C$	$g-V$	$g-r$	$g-i$	$C-M$	$M-V$	$M-T_1$	$M-T_2$
1.0	0.422	0.908	0.124	0.149	0.277	0.266	0.189	0.546	1.074
1.5	0.414	0.892	0.121	0.137	0.259	0.235	0.184	0.534	1.056
2.0	0.408	0.880	0.119	0.127	0.245	0.213	0.181	0.526	1.041
3.0	0.401	0.866	0.116	0.116	0.229	0.193	0.177	0.517	1.024
4.0	0.399	0.860	0.115	0.113	0.223	0.186	0.176	0.514	1.018
5.0	0.399	0.859	0.115	0.113	0.222	0.185	0.177	0.514	1.017
6.0	0.399	0.859	0.116	0.114	0.224	0.187	0.177	0.515	1.019
8.0	0.403	0.864	0.117	0.119	0.231	0.194	0.179	0.520	1.027
10.0	0.407	0.870	0.119	0.125	0.239	0.202	0.182	0.525	1.035
12.5	0.412	0.877	0.121	0.133	0.249	0.212	0.185	0.532	1.046
15.0	0.416	0.884	0.123	0.140	0.259	0.222	0.188	0.538	1.057

© Royal Astronomical Society • Provided by the NASA Astrophysics Data System

2005MNRAS.361..725B

Table A7. Template model for Im galaxies.

		Johnson							
Age [Gyr]	Bol	Bol − *V*	*U* − *V*	*B* − *V*	*V* − *R*	*V* − *I*	*V* − *J*	*V* − *H*	*V* − *K*
1.0	−20.298	−0.929	−0.074	0.299	0.450	0.895	1.379	2.001	2.134
1.5	−20.743	−0.901	−0.030	0.321	0.467	0.920	1.412	2.036	2.171
2.0	−21.043	−0.883	0.001	0.337	0.479	0.939	1.435	2.062	2.199
3.0	−21.481	−0.861	0.046	0.360	0.497	0.967	1.470	2.101	2.240
4.0	−21.800	−0.847	0.080	0.377	0.510	0.988	1.497	2.131	2.272
5.0	−22.040	−0.838	0.106	0.390	0.520	1.004	1.518	2.153	2.296
6.0	−22.236	−0.832	0.127	0.401	0.529	1.018	1.534	2.172	2.316
8.0	−22.547	−0.822	0.161	0.419	0.543	1.039	1.561	2.202	2.348
10.0	−22.791	−0.816	0.188	0.432	0.553	1.056	1.583	2.226	2.373
12.5	−23.030	−0.811	0.214	0.446	0.564	1.073	1.604	2.249	2.398
15.0	−23.229	−0.807	0.236	0.457	0.573	1.087	1.622	2.269	2.419

	Cousins		Gunn			Washington			
Age [Gyr]	*V* − R_C	*V* − I_C	*g* − *V*	*g* − *r*	*g* − *i*	*C* − *M*	*M* − *V*	$M - T_1$	$M - T_2$
1.0	0.306	0.702	0.077	−0.028	0.022	−0.012	0.125	0.390	0.807
1.5	0.318	0.722	0.082	−0.009	0.048	0.016	0.132	0.406	0.834
2.0	0.327	0.736	0.086	0.004	0.067	0.037	0.137	0.418	0.854
3.0	0.340	0.757	0.092	0.024	0.095	0.064	0.145	0.436	0.883
4.0	0.350	0.773	0.096	0.039	0.116	0.084	0.150	0.449	0.906
5.0	0.357	0.786	0.099	0.050	0.132	0.100	0.154	0.459	0.922
6.0	0.363	0.796	0.101	0.060	0.145	0.113	0.158	0.467	0.936
8.0	0.373	0.812	0.106	0.075	0.166	0.134	0.163	0.481	0.959
10.0	0.381	0.825	0.109	0.086	0.183	0.150	0.168	0.491	0.976
12.5	0.389	0.838	0.112	0.098	0.200	0.166	0.172	0.502	0.994
15.0	0.395	0.848	0.115	0.108	0.213	0.179	0.176	0.510	1.009

types. All the models assume a total *stellar* mass $M_{gal} = (M_{bulge} + M_{disc} + M_{halo}) = 10^{11}$ $M_\odot$ at 15 Gyr (see footnote 6 for an operational definition of M_{gal}).

Full details of the photometric systems (i.e. band wavelength and magnitude zero-points) can be obtained from Table 1.

Each table is arranged in two blocks of data. The description of the entries in the upper block is the following.

Column 1 – Age of the galaxy, in Gyr.

Column 2 – Absolute magnitude of the model, in bolometric. For the Sun, we assume $Bol_\odot = 4.72$.

Column 3 – Bolometric correction to the Johnson *V*-band. The adopted solar value is $(Bol - V)_\odot = -0.07$.

Column 4–10–Integrated broad-band colours in the Johnson system (filters *U*, *B*, *V*, *R*, *I*, *J*, *H*, *K*);

The lower block of data has the following entries.

Column 1 – Age of the galaxy, in Gyr.

Column 2–3 – Integrated colours in the Johnson/Cousins system (filters R_C and I_C).

Column 4–6 – Integrated colours in the Gunn system (filters *g*, *r*, *i*), with the *g* − *V* colour allowing a self-consistent link to the Johnson photometry.

Column 7–10 – Integrated colours in the Washington system (filters *C*, *M*, T_1, T_2), with the *M* − *V* colour linking the Johnson photometry.

It may also be worth recalling that a straightforward transformation of our photometry to the Sloan SDSS photometric system (extensively used in recent extragalactic studies) can be carried out according to the set of equations in Fukugita et al. (1996, their equation 23).

To allow easier graphical display and interpolation of the data, all the magnitudes and colours in Tables A1–A7 are reported with three-digit nominal precision; see, however, Section 2 and 4 for a more detailed discussion of the real internal uncertainty of synthetic photometry in our models.The entire theoretical data base is publicly available at the author's Web site: http://www.bo.astro.it/∼eps/home.html.

This paper has been typeset from a TEX/LATEX file prepared by the author.

© Royal Astronomical Society • Provided by the NASA Astrophysics Data System